EUROP[redacted]ARCH

CERN-PPE-94-140

CERN-PPE/94-140
24 August 1994

Low-mass lepton-pair production in p-Be collisions at 450 GeV/c

T.Åkesson[3,a], S. Almehed[6], A.L.S. Angelis[20,b], J. Antos[3,c], H. Atherton[3], P. Aubry[8], H.W. Bartels[4], G. Beaudoin[8], J.M. Beaulieu[8], H. Beker[3,d], O. Benary[18], D. Bettoni[3,e], V. Bisi[19], I. Blevis[3,f], H. Bøggild[3,g], W.Cleland[12], M. Clemen[12], B. Collick[12], F. Corriveau[7], S. Dagan[18], K. Dederichs[3,h], P. Depommier[8], N. DiGiacomo[5,w], S. DiLiberto[13], J.R. Dodd[20,i], B. Dolgoshein[10], A. Drees[4], S. Eidelman[11], H. En'yo[3,j], B. Erlandsson[17], M.J. Esten[20], C.W. Fabjan[3], P. Fischer[4], A. Gaidot[15], F. Gibrat-Debu[15], P. Giubellino[19], P. Glässel[4], U. Goerlach[3,k], Y. Golubkov[10,x], R. Haglund[6], L.A. Hamel[7,l], H. van Hecke[5], V. Hedberg[3,a], R. Heifetz[18], A. Holscher[4], B. Jacak[5], G. Jarlskog[6], S. Johannson[6], H. Kraner[2], V. Kroh[4], F. Lamarche[7,m], C. Leroy[7,l], D. Lissauer[2,18], G. London[15], B. Lorstad[6], A. Lounis[8], F. Martelli[19,n], A. Marzari-Chiesa[19], M. Masera[19], M.A. Mazzoni[3,d], E. Mazzucato[7,o], M.L. McCubbin[20,p], N.A. McCubbin[14], P. McGaughey[5], F. Meddi[13], U. Mjörnmark[6], M.T. Muciaccia[1], S. Muraviev[9], M. Murray[12], M. Neubert[4], P. Nevski[10], S. Nilsson[17], L. Olsen[2], Y. Oren[18], J.P. Pansart[15], Y.M. Park[12], A. Pfeiffer[4], F. Piuz[3], V. Polychronakos[2], P. Pomianowski[12], G. Poulard[3], M. Price[3], D. Rahm[2], L. Ramello[19,q] L. Riccati[19], G. Romano[16], G. Rosa[13,r], L. Sandor[3,s], J. Schukraft[3], M. Sekimoto[3,t], M. Seman[3,c], A. Shikanian[9], A. Shmeleva[9], V. Sidorov[11], S. Simone[1], Y. Sirois[7,m], H. Sletten[3], S. Smirnov[10], W. Sondheim[5], H.J. Specht[4], E. Stern[12], I. Stumer[2], A. Sumarokov[10,z], J.W. Sunier[5,+], V. Tcherniatin[10,y], J. Thompson[12], V. Tikhomirov[9], A. Vanyashin[10,y], G. Vasseur[15], R.J. Veenhof[3,u], R. Wigmans[3,v], W.J. Willis[3,i], P. Yepes[7]

Abstract

We report on the production of low-mass electron pairs and muon pairs in p-Be collisions at 450 GeV/c at the CERN SPS. For both electron and muon pairs the low-mass spectrum can be explained satisfactorily by lepton pairs from hadronic decays, and there is no need to invoke any "unconventional" source. The normalisation of the major hadronic sources is set by the data. The upper limit, at 90% confidence level, on any new source of lepton pairs is $\sim$ 20% of the hadronic decay contribution for muons, and $\sim$ 40% for electrons.

(to be submitted to Zeit. Phys. C)

[1] University of Bari and INFN, I-70100 Bari, Italy
[2] Brookhaven National Laboratory, Upton, NY 11973, USA
[3] CERN, CH-1211 Geneva 23, Switzerland
[4] University of Heidelberg, D-69120 Heidelberg, Germany
[5] Los Alamos National Laboratory, Los Alamos, NM87544, USA
[6] University of Lund, S-223 62 Lund, Sweden
[7] McGill University, Montreal, PQ H3A 2T8 Canada
[8] University of Montreal, Montreal, PQ HC3 3J7 Canada
[9] Lebedev Institute of Physics, RU-117924 Moscow, Russia
[10] Institute of Physics and Engineering, RU-115409 Moscow, Russia
[11] Institute of Nuclear Physics, RU-630090 Novosibirsk, Russia
[12] University of Pittsburgh, Pittsburgh PA 15260, USA
[13] University of Rome 'La Sapienza' and INFN, I-00185 Rome, Italy
[14] Rutherford Appleton Laboratory, Didcot OX11 0QX, UK
[15] DAPNIA, CE Saclay, F-91191 Gif-sur-Yvette, France
[16] University of Salerno and INFN, I-84100 Salerno, Italy
[17] University of Stockholm, S-11346 Stockholm, Sweden
[18] University of Tel Aviv, Ramat Aviv 69978, Israel
[19] University of Turin and INFN, I-10100 Turin, Italy
[20] University College London, London WC1E 6BT, UK
[a] Now at: University of Lund, S-223 62 Lund, Sweden
[b] Now at: University of Geneva, CH-1211 Geneva 4, Switzerland
[c] Visitor at CERN from Slovak Academy of Sciences, SQ-04353 Kosice, Slovak Republic
[d] Now at: University of Rome 'La Sapienza' and INFN, I-00185 Rome, Italy
[e] Now at: University of Ferrara and INFN, I-44100 Ferrara, Italy
[f] Visitor at CERN from Weizmann Institute, Rehovot, Israel
[g] Visitor at CERN from Niels Bohr Institute, DK-2100 Copenhagen Ø, Denmark
[h] Visitor at CERN from Ludwig-Maximilians-Universität, D-W-8000 München, Germany
[i] Now at: University of Columbia, Nevis Labs., NY 10533, USA
[j] Now at: University of Kyoto, Kyoto 606, Japan
[k] Now at: DESY, D-W-2000 Hamburg 52, Germany
[l] Now at: University of Montreal, Montreal, PQ HC3 3J7 Canada
[m] Now at: Ecole Polytechnique, F-91128 Palaiseau, France
[n] Now at: University of Urbino, I-61029 Urbino, Italy
[o] Now at: DAPNIA, CE Saclay, F-91191 Gif-sur-Yvette, France
[p] Now at: University of Liverpool, Liverpool L69 3BX, UK
[q] Now at: Politecnico of Milan, I-20100 Milan, Italy
[r] Now at: University of Salerno and INFN, I-84100 Salerno, Italy
[s] Now at: Slovak Academy of Sciences, SQ-04353 Kosice, Slovak Republic
[t] Visitor at CERN from Institute of Nuclear Study, Tokyo 188, Japan
[u] Visitor at CERN from NIKHEF-H, NL-1009 DB Amsterdam, the Netherlands
Now at: LIP, P-1000 Lisboa, Portugal
[v] Now at: Texas Tech. University, Lubbock TX 79409, USA
[w] Now at: SAIC, San Diego, USA
[x] Now at: Moscow State University, RU-117234 Moscow, Russia
[y] Now at: Brookhaven National Laboratory, Upton, NY 11973, USA
[z] Now at: Institute of Physics, Acad. Sinica, Taipei 11529, Taiwan
[+] Deceased

1 Introduction

The production of low-mass lepton-pairs ($m_{pair} < m_\rho$) in hadronic collisions has been measured in several experiments, stretching back over more than a decade [1]. Despite this considerable amount of experimental effort and data, it has remained unclear whether the production of these pairs matches that expected from "conventional sources", i.e. hadronic decays, hadronic bremsstrahlung of virtual photons, and Drell-Yan. This uncertainty has been due in large part to inadequate knowledge of the relevant hadronic production cross-sections and of the decay modes into lepton pairs.

Clearly this issue should be settled, since any significant deviation from the level implied by conventional sources could have important implications for the hadronisation process [2]. Furthermore, lepton pairs have been suggested as a signature for quark-gluon plasma formation in relativistic heavy-ion collisions [3]: it is essential then to understand their production level in ordinary hadronic collisions.

In this paper the production of electron and muon pairs, produced in 450 GeV/c p-Be collisions ($\sqrt{s} \simeq 29\,\mathrm{GeV}$) in the central rapidity region, is compared to the expectation from conventional sources. The most important features of the experimental approach are:

- the analysis of both electron pairs and muon pairs, emphasising different aspects of the detector, producing two essentially independent measurements of lepton pairs;
- the measurement of photons as well as charged leptons, affording direct measurement of certain Dalitz decay modes;

Other noteworthy points are:

- a double measurement of the momentum (or energy) of both muons and electrons;
- electron identification by both transition radiation and calorimetry;
- a measurement of the total charged multiplicity of the event.

The main result is that low-mass lepton pairs, produced centrally at $\sqrt{s} \simeq 29\,GeV$, can be accounted for by lepton pairs from the decay of hadrons, and there is no need for any "unconventional" source. Upper limits on any new source are presented.

The plan of this paper is as follows. In section 2 we describe the apparatus, triggering, and data-taking, followed by the event reconstruction and selection in section 3. The analysis is presented in section 4, and in section 5 results are summarised and conclusions are drawn.

2 Apparatus, Triggering, and Data-Taking.

2.1 Beam and Target

The study of low-mass lepton pairs was one of the prime motivations of the HELIOS experiment, and so the suppression of e^+e^- pairs from conversions was a key feature of the design. Accordingly, we have used a 4 cm long (10% interaction length) Be wire target of only 125 μm diameter, in order to minimize the radiation length traversed by photons from the decay of hadrons produced in the interaction.

A special 450 GeV/c proton "micro"-beam was developed for the HELIOS experiment to match the wire target. This beam has excellent momentum resolution ($\delta p/p \sim 0.1\%$), a transverse diameter less than 50 μm and divergence $\sim 0.2\,\mathrm{mrad}$ at the target. The intensity was $\sim 10^6$ per burst. The targeting of the beam on to the wire worked reliably and stably throughout the experiment.

2.2 Apparatus

The HELIOS spectrometer is situated in the H8 beam line of the CERN SPS North Area. An overview of the apparatus is shown in Figure 1a. The main components are

the electron spectrometer and muon spectrometer covering the forward region $\theta_{LAB} < 6°$ (i.e. $\eta_{LAB} > 2.9; \eta_{ppCM} > -0.4$), and calorimetric energy measurement over the full solid angle.[1] The characteristics of the main components are given in Table 1, together with references where more details may be found. Features of particular relevance to this analysis are described in the sections on triggering and reconstruction.

2.3 Triggering

Incoming protons are defined by three small scintillation counters (SCbeam) placed 270 cm and 140 cm upstream of the target. Two larger scintillators, with central holes, act as a halo counter (SChalo) and were used in veto. A "valid beam" signal, VB, is $SCbeam.\overline{SChalo}$, combined with suitable timing protection to ensure that there is no second beam particle within a −350nsec to +500nsec "before-after" window. The interaction pre-trigger, PRE, consists of VB in coincidence with a charged multiplicity ≥ 3 as seen by the Si-pad detector (Table 1). Further triggering steps are now required to select electron pair and muon pair samples.

2.3.1 Electron Trigger

The electron trigger performs the two tasks of identifying electrons and rejecting those from conversions. Very extensive discussions of the electron trigger may be found in theses from the HELIOS experiment [9]. For the data described in this paper, two isolated trigger electrons are required.

2.3.1.1 First Level Electron Trigger

The first level of the electron trigger uses information from the $18X_0$ electromagnetic (e.m.) section of the Uranium Liquid-Argon Calorimeter (ULAC) [10] in combination with information from the Transition Radiation Detector (TRD) [8, 9] to identify electrons. The e.m. section of the ULAC has a central hole of 5 cm diameter ($\theta < 6$ mrad) so that small-angle secondaries do not create showers which would overlap with showers from wider angle secondaries. The granularity of the read-out is $2 \times 2\,\mathrm{cm}^2$ towers, formed by longitudinal summing of the $2 \times 2\,\mathrm{cm}^2$ pads of each read-out cell. For trigger purposes, the towers are combined to make 256 "super-pad" sums, increasing in size from $4 \times 6\,\mathrm{cm}^2$ close to the beam to $8 \times 12\,\mathrm{cm}^2$ at the outer edge. The electron trigger requires an energy deposit in a super-pad above a threshold of 2.5 GeV. The tower signals are distributed to the super-pad sums so that the super-pads "overlap". This ensures that there is no trigger inefficiency whenever an above-threshold signal is split between two towers into two sub-threshold signals.

Each of the 8 TRD chambers is readout in both x (60 channels) and y (152 channels). For trigger purposes these x and y signals were summed over all 8 TRD chambers and combined into 24 x "groups" and 30 y "groups" matching the ULAC super-pads. A TRD group is "ON" if any sum in the group exceeds 7 "clusters", where each cluster is ~ 5 keV. A transition radiation photon deposits ~ 5 keV in a single chamber; a minimum ionising particle deposits ~ 3 keV.

The first level trigger identifies an electron candidate by requiring a coincidence between a ULAC super-pad and the corresponding TRD x and y groups.

---

[1] We use a right-handed co-ordinate system with z along the beam direction and y pointing vertically upwards.

Sub-Detector	Main Characteristics	References
Electron Spectrometer:		
Si-Pad	400 Si "pads", situated 15cm down-stream of target. Pad size varies from $0.2 \times 2\,mm^2$ close to the beam direction to $2 \times 7\,mm^2$ at the outer perimeter of the detector. There is a central hole (diameter $\sim$ 0.5mm) to allow the beam to pass through.	[4, 5]
Si-strips	3 planes of Si strip detectors, at 6, 12, and 18cm from the target. All strips are vertical and on a 25 μm pitch. The read-out uses capacitive charge-division.	[5]
Drift Chambers (DC)	DC1 : x,y,u,v,x,y planes. Total of 384 wires. DC2 : y,x,u,v,y,w planes. Total of 480 wires. DC3 : y,x,u,v,w planes. Total of 540 wires. The DC system has an angular resolution of 1.5 mrad. For reconstructed tracks in the multiplicities typical of high-energy pBe collisions, the two-track efficiency is $\sim$ 70% for a track separation of 5mm, rising to full efficiency at around 1cm.	[6, 15]
MAGCAL	Dipole magnet with calorimetrised yoke. p_T kick $\sim$ 60 MeV/c in horizontal (x-z) plane.	[7]
TRD	8 module Transition Radiation Detector. Each module is a 64mm thick radiator of 250 polypropylene foils, followed by a drift chamber filled with 95/5 Xenon/Isobutane and equipped with x and y read-out, using "cluster-counting". The TRD is fully efficient at $\gamma \sim 4000$. For isolated 5 GeV particles, the hadron rejection is $\sim 10^3$ for an electron efficiency of 90%. In the multiplicities typical of high energy pBe collisions, the hadron rejection is degraded by a factor of 10 to 20.	[8, 9, 16]
Scint-pad	Plane of 80 scintillator "pads" positioned between drift chamber (DC3) and calorimeter (ULAC). Pad size varies from $2 \times 4\,cm^2$ close to the beam direction to $10 \times 10\,cm^2$ at the outer perimeter of the detector. There is a central hole to allow the non-interacting beam to pass through.	
ULAC	Uranium Liquid Argon Calorimeter. Electro-magnetic section is 36 cells; total of $18X_0$. Each cell is (thicknesses in mm): U(1.7);Liq. Argon(2);Read-out plane(1.6); Liq. Argon(2) The granularity of the electro-magnetic section read out is $2 \times 2\,cm^2$ pads. Resolution: $11.6\%/\sqrt{E(GeV)}$ Hadronic section: 4.5λ	[10]
BEAM+VETO	Uranium-Scintillator calorimeter: 5.8λ	[7]
BOX+WALL	Uranium-Scintillator calorimeter covering wide angle region.	[7]
Muon Spectrometer:		
Proportional Chambers (PC)	PC0 : x,u,v planes. Total of 1536 wires. PC1 : x,u,v planes. Total of 1536 wires. PC2 : x,y,u,v,y,x planes. Total of 2688 wires. PC3 : x,y,u,v,y,x planes. Total of 5696 wires. PC4 : x,y,u,v,y,x planes. Total of 5824 wires. PC5 : x,x,y,u planes. Total of 5696 wires. PC6 : x,y,v,x planes. Total of 5952 wires.	[11, 12, 14]
Muon Magnet	Large aperture (1.6m diameter) super-conducting dipole magnet with p_T kick $\sim$ 1.2 GeV/c in horizontal (x-z) plane.	[11, 14, 13]
Hodoscopes H2,H3	Each hodoscope consists of two layers of scintillators; each layer has 10(H3) or 11 (H2) rows. Each row contains two horizontal scintillator slabs, $3 \times 0.24\,m^2$.	see section 2.3.2

Table 1: Summary of main sub-detectors

2.3.1.2 Second Level Electron Trigger

The second level of the electron trigger rejects conversions, by correlating the first-level ULAC/TRD information with information from the Si-pad detector [4] positioned 15cm downstream of the target. The essential idea is that the Si-pad detector will register no charged particles ("0") for a photon conversion occurring down-stream of the pad detector, a single charged particle signal ("1") for a single electron of the type of interest, and a two-charged particle signal ("2") for a conversion which occurs upstream, i.e. in the target or first two Si-strip detectors.

The Si-pad detector comprises 400 pads, varying in size from $0.2 \times 2\,\mathrm{mm}^2$ near the centre to $2 \times 7\,\mathrm{mm}^2$ at the perimeter. The longer (horizontal) direction allows for the magnetic bending as the particle passes from Si-pad to TRD. The pad area is small to minimize the chance of an overlap with a charged hadron. The trigger signals available from each pad of the detector are "Single", corresponding to a signal greater than one minimum ionising particle (mip), and "Double", corresponding to the signal summed from the pad, the one above it and the one below it being greater than 2 mips. The purpose of this vertical summing is to recognise conversions with small opening angle in the vertical direction. There is no such summing in the horizontal direction in which the individual pads are much longer.

For each electron candidate passing the first level trigger, the second level trigger examines those Si pads which project on to the ULAC/TRD coincidence, and requires that at least one pad has the "Single" signal and no Si-pad vertical group has its "Double" signal set. (The number of Si-pads overlapping a ULAC super-pad varies from 5 at large angles to 18 in the region closest to the beam.)

Photon conversions downstream of the Si-pad detector can still satisfy the electron trigger if a charged particle passes through one of the Si-pads to satisfy the "Single" requirement. To reject conversions occurring after the magnet, a Scintillator Pad detector (Table 1) consisting of a plane of 80 scintillators was installed between the TRD and the ULAC. An electron trigger candidate is rejected if the Scintillator Pad associated with a ULAC super-pad gives a pulse-height > 2 mips.

The pair trigger requires that there be at least two surviving electron candidates. One possible contribution to the pair trigger is a single electron which strikes the ULAC in towers which contribute to two adjacent ULAC super-pads, with all subsequent trigger requirements being satisfied for each ULAC super-pad. To guard against this, the final stage of the trigger implements a veto scheme which rejects a pair candidate if it comes from adjacent ULAC super-pads, with the consequence that the two electron candidates must have a small solid-angle isolation, corresponding to at least 5cm separation at the ULAC.

2.3.2 Muon Trigger

The muon trigger is less complex than the electron trigger. The muon spectrometer (Figure 1a) consists of seven sets of Proportional Chambers (PC0-PC6) with a total of 32 planes [11, 12], a large aperture super-conducting magnet (p_T-kick in the horizontal plane of 1.22 GeV/c) [11, 13], and two double-layer scintillator hodoscopes, H3 and H2, on either side of an 80cm Iron wall. Most of these components were used in the NA3 or NA4 experiments. Further details of the spectrometer as used in this experiment can be found in [14], with the exception of the hodoscope arrangement which is described below.

Each scintillator hodoscope, H3 and H2, is made up of Front and Back layers, and each layer consists of 10(H3) or 11(H2) rows, Figure 1a and 1c. The H3 rows are offset

with respect to H2 rows by half a row width (12cm). Each row contains two (Left and Right) horizontal scintillator slabs. Each scintillator slab measures $3 \times 0.24\,m^2$, and is read out by a single photomultiplier tube at one end. In the Front layers the Left and Right slabs abut against each other to give a combined horizontal coverage of 6m. A substantial fraction of the slabs were used in earlier experiments, are over ten years old, and have a poor efficiency ($\sim$ 50%) for a hit far from the photomultiplier. These older slabs were used in the Back layers and, to recover good efficiency, the Left and Right slabs were overlapped by 2m, to give a combined horizontal coverage of 4m.

The muon trigger has two levels : a pre-trigger from H3 and H2, and a chamber trigger which uses vertical-wire planes in PC3, 5, and 6, and which is part of the general second-level triggering.

Trigger rows were defined in each hodoscope by an 'OR' of the four slabs in each row, i.e. Front layer/Left slab, Front/Right, Back/Left, Back/Right. However, Monte-Carlo studies showed that opposite-sign muon pairs would give one hit in the Left slabs and one in the Right for the two rows in H3 (in front of the Iron wall) immediately above and below the beam axis. So for these two rows in H3 the Left and Right scintillators in the Back layer were not overlapped (2m long slabs were used instead), and the distinction between Left and Right was maintained in the trigger for both Front and Back layers.

The muon pre-trigger requires an H3 trigger row to be in coincidence with either of the two H2 trigger rows which overlap with it.

The second level of the muon trigger looks for tracks in the trigger planes of PC3, 5, and 6. These chambers are downstream of the muon magnet, and are positioned such that PC5 is half way between PC3 and PC6 (see Figure 1a). The track requirement is that there be a PC5 hit at the position predicted by a PC3/PC6 combination. For the di-muon trigger two such tracks are required.

2.4 Data-taking

The results described in this paper were obtained from the analysis of data taken during the SPS Fixed Target running period in the second half of 1989. The typical beam intensity was around $0.5 - 1.0\,10^6$ protons on target per 2.4 second burst. With this beam intensity the di-electron trigger rate was $\sim$ 15 per burst and the di-muon trigger rate $\sim$ 10 per burst. Other triggers were also taken at the same time, mainly to monitor detector performance. The over-all live-time of the data acquisition system with these trigger rates was around 50%.

A total of $5.4\,10^6$ electron pair triggers and $4.2\,10^6$ muon pair triggers were recorded.

3 Event Reconstruction and Selection

3.1 Pile-up rejection

Prior to off-line event reconstruction, the data were checked for correct performance of the detectors and data acquisition. Also, cuts were applied to ensure that no other interaction had taken place within $-1.5 \rightarrow +2.0 \mu sec$ of the triggered event, using the timing of hits in various scintillation counters and the total energy measured by the calorimeters. The time window is dictated essentially by the ULAC response time. This pile-up rejection complements the timing protection done at the trigger level. (Section 2.3)

About 88% of triggered events passed these initial selection criteria.

3.2 Electron reconstruction

The off-line electron reconstruction consists of shower reconstruction in the electromagnetic (e.m.) section of the ULAC, the matching of a reconstructed track in the Drift chambers to the ULAC shower, and checks that the pair of interest satisfies the trigger criteria.

Showers are reconstructed in the e.m. section of the ULAC by searching for localised energy deposits in a 3x3 array of towers (i.e. $6 \times 6\,\mathrm{cm}^2$). Off-line, the ULAC e.m. information is available separately for the front $6X_0$ and back $12X_0$, and it is required that the energy reconstructed in the front be at least 0.6 GeV and in the back at least 1.0 GeV. The centre of a reconstructed shower is required to lie in the range 10cm to 35cm from the beam axis, corresponding to an angular acceptance of 25 to 87.5 mrad. In order to reduce contamination from nearby showers, the energy in the block of 3x3 towers must be at least 35% of the energy in the block of 5x5 towers in which it is embedded.

Track reconstruction in the Drift Chambers (DC1,2,3; Figure 1a) uses a starting "road" defined by the combination of a ULAC shower and a matching track in the TRD. This puts a premium on finding electron tracks of high quality, to the slight detriment of reconstructing nearby tracks e.g. from conversions; we return to this point later. The DC reconstructed track, extrapolated to the ULAC, is required to match the ULAC shower within 1cm. (The centre of e.m. showers is determined with $\sigma \sim 4$mm.)

Of the original $4.8\,10^6$ events which survive the initial pile-up rejection, only 183k have two reconstructed DC tracks, and only 80k of these have both DC tracks matching the ULAC shower to within 1cm. These candidate electrons are required to satisfy the on-line electron trigger. Using the Si-strip detectors (Figure 1b and Table 1) the z position of the interaction vertex can be determined with $\sigma \sim 400$ μm. It is then required that the electron trajectory should match the triggering Si pad to within 600 μm. The ratio of the ULAC energy to the reconstructed momentum for the surviving electron candidates is shown in Figure 2. The pronounced peak around $E/p = 1$ shows that the candidates are indeed mainly electrons. At this stage it is required that $0.6 < E/p < 1.4$, satisfied by $\sim$ 20k events.

As mentioned above, the "road" method used in the DC reconstruction results in some loss of finding nearby conversion partners. This is rectified as follows. We define a horizontal band in the ULAC of width $\pm$3cm around the impact point of the reconstructed track. Any ULAC energy deposition (energy $E_{partner}$) in this band is then tested as a possible conversion partner. (These energy depositions satisfy much looser requirements than reconstructed showers.) Because conversions have zero opening angle, the conversion partner starts with the same angle as the reconstructed track. For conversions which take place before the magnet we can use this angle and the position of the ULAC energy deposition to define the trajectory of the possible partner through the magnet, and hence its momentum, $P_{partner}$, can be calculated. We also require at least two TRD clusters in the vicinity of the partner trajectory, to enhance the likelihood of a real electron track. The distribution of $E_{partner}/P_{partner}$, with the TRD cluster requirement applied, is shown in Figure 3. There is a broad peak around 1, indicating that there are indeed conversion partners which are not reconstructed in the Drift Chambers. The event is rejected if $0.25 < E_{partner}/P_{partner} < 1.75$ and there are at least two TRD clusters in the vicinity of the trajectory.

The final di-electron data sample, with $M_{ee} > 50$ MeV and a distance at the ULAC e.m of at least 6 cm between shower centres, consists of 4462 events, of which 3842 are e^+e^- and 287 e^+e^+ and 333 e^-e^-. The mass spectra of the final e^+e^-, e^+e^+, and e^-e^-

samples are shown in Figure 4. The sharp peak in e^+e^- at $M < 120\,\mathrm{MeV}$ is the tail of the π^0 Dalitz decay. The other immediately noticeable feature is the peak in the ρ/ω region. This plot will be discussed in detail in section 4.

3.3 Muon reconstruction

Reconstruction of di-muon candidates proceeds by first reconstructing tracks using the Proportional Chambers (PC) of the muon spectrometer, and requiring corresponding hits in the hodoscopes H3 and H2. Of the $4.2\,10^6$ di-muon triggers recorded, $3.7\,10^6$ pass initial event selection (section 3.1), and $1.7\,10^6$ have two tracks fully reconstructed in the PC's of the muon spectrometer with $p > 6\,\mathrm{GeV/c}$. The $\mu^+\mu^-$ invariant mass spectrum of a sample of these $1.7\,10^6$ events is shown in Figure 5. For this figure the mass is calculated from muon spectrometer variables, correcting for energy loss in the upstream calorimeters. A broad shoulder/peak is visible in the ρ/ω region. The data also contain a few hundred J/ψ, shown in the inset of Figure 5.

The great majority of these tracks are not prompt muons from the primary interaction, but muons from π and K decay in the 4m path before the ULAC, or muons from the decay of particles produced in the calorimeter. The reconstructed vertex of the two tracks shows a strong peak in the last interaction length of the calorimeters. This peak is correlated with a relatively high multiplicity of hits in PC0 and PC1, which are immediately downstream of the calorimeters and upstream of the muon magnet, caused by leakage of shower particles from the calorimeters. This high hit multiplicity is not seen in the PC's downstream of the muon magnet because the magnet sweeps away the relatively soft shower particles. Events are discarded if any plane in PC0 or PC1 has more than 5 hits. After this cut, the vertex distribution shows no peak in the calorimeters.

The major rejection of background comes from matching the track reconstructed in the muon spectrometer to a track reconstructed in the electron spectrometer. For this purpose muon spectrometer tracks are extrapolated back into the electron spectrometer, assuming that the muons originate from the target. The muon spectrometer track has in general suffered a change in direction and a displacement as a result of multiple scattering in the calorimeters between the two spectrometers. The direction of the extrapolated track in the electron spectrometer is found by maximum likelihood, using the target constraint and the usual small angle multiple scattering approximation, including of course the correlation between scattering angle and displacement. Energy loss in the calorimeters is taken into account in the extrapolation procedure.[2] The extrapolated track is matched to a drift chamber track by requiring:

1. that, as a preliminary filter, the muon track, extrapolated without the target origin constraint back to the x-y plane at the target, is < 75cm away from the beam axis;
2. that the distance, d, between the extrapolated muon-spectrometer track (momentum p_μ, after energy loss correction) and the electron-spectrometer track (momentum p_{DC}) satisfies $d < 50\mathrm{cm}/p_\mu(\mathrm{GeV})$ at z=300cm ;
3. that $\mid p_\mu - p_{DC} \mid < 3\sigma_{DC}(p_\mu)$, where $\sigma_{DC}(p_\mu)$ is the momentum resolution of the electron spectrometer evaluated at momentum p_μ;
4. that the charges in the muon and electron spectrometers are the same.

The matching cuts were optimised by studying "accidental" matches, defined to be *opposite* sign tracks satisfying all other matching criteria. In particular, such studies led

[2] The calorimeters comprise $\sim 13\lambda$ and $\sim 300X_0$. A 15 GeV muon loses about 4 GeV in traversing the calorimeters. This loss rises to about 5 GeV for a 50 GeV muon as bremsstrahlung and pair-production become more significant.

to the requirement that the distance from the beam axis at the target be less than 75cm.

To check the estimation of the energy loss correction, we have studied the mean and standard deviation of the distribution of $p_\mu - p_{DC}$. The standard deviation is shown in Figure 6a as a function of p_μ. The contributions to the deviation are the resolutions of the electron and muon spectrometers, and any fluctuation in the energy loss itself. The momentum resolution of the muon spectrometer is $\sigma(p)/p = 3.10^{-4}p(GeV/c)$, which is more than an order of magnitude better than that of the electron spectrometer. So the contribution from the spectrometers is completely dominated by the electron spectrometer resolution, which is shown as the solid line in Figure 6a. This agrees well with the measurements, from which we infer that any fluctuation in the energy loss is at most 1-2% of the momentum. The mean of $p_\mu - p_{DC}$ is plotted in Figure 6b. This shows a systematic shift away from zero for large momentum. The shift is however much smaller than the electron spectrometer resolution and is also seen in data taken with calorimeters removed [15]. The agreement between the data sets with and without the calorimeters implies that energy loss correction is good to around 1%.

During the course of the experiment we observed a gradual loss of efficiency of the drift chambers in the region around the beam direction, due to the very high flux of produced particles there. To avoid this region we have required both matched drift chamber tracks to have $\theta > 10\,\mathrm{mrad}$. The upper limit for the muon spectrometer acceptance is 70 mrad, but the DC read-out has some gaps above 60 mrad. Since there are very few events with muons above 60 mrad, we have required both matched DC tracks to have $\theta < 60\,\mathrm{mrad}$, rather than work in a region with patchy read-out efficiency.

The best choice of kinematic parameters is to take the direction from the matched track in the electron spectrometer, but the momentum from the measurement in the muon-spectrometer, corrected for energy loss in the calorimeters. (As discussed above, the momentum resolution of the muon spectrometer is far superior to that of the electron spectrometer, and the fluctuation in the energy loss is small.) In this way we achieve a resolution on the di-muon mass of 30 MeV at ~ 1 GeV, to be compared to ~ 100 MeV which is the best that can be achieved using just the muon spectrometer and target origin constraint. The final selection of events is made by cutting away the edges of the acceptance by requiring $0.25 < y < 1.5, p_T < 2\,\mathrm{GeV/c}$, and $|\, cos\theta^* \,| < 0.75$, where y is the c.m rapidity of the di-muon system, p_T is its transverse momentum, and θ^* is the decay angle in the di-muon centre of mass.

The final sample consists of 11888 events, of which 9045 are $\mu^+\mu^-$, 1939 are $\mu^+\mu^+$, and 904 are $\mu^-\mu^-$. The excess of $\mu^+\mu^+$ compared to $\mu^-\mu^-$ is due to both charge conservation and asymmetric acceptance. The mass spectra of the final samples are shown in Figure 7. The ρ/ω and φ resonances are clearly visible.

A very thorough discussion of the muon reconstruction procedure, as well as of the physics analysis, may be found in [15].

4 Analysis and Results

4.1 Kinematics and acceptance.

The di-lepton mass-spectra of the final event samples are shown in Figure 4 and Figure 7.

The detector acceptance and event selection procedures described in section 3 result in the data lying in the kinematic regions:

	y	$cos\theta^*$
electron pairs	-0.25 to $+1.25$	-0.75 to $+0.75$
muon pairs	$+0.25$ to $+1.50$	-0.75 to $+0.75$

where y is the rapidity of the lepton pair in the pp centre of mass, and θ^* is the decay angle in the di-lepton rest frame. So the data lie in the "central" rapidity region.

Within the above kinematic regions the acceptance is correlated between the mass and p_T of the lepton pair, basically as a result of the acceptance in polar angle. (The acceptance is estimated by Monte-Carlo, as described in 4.2.2.) For example, muon pairs with mass $< 300\,\mathrm{MeV}$ have very low acceptance for $p_T < 500\,\mathrm{MeV/c}$, whilst for muon masses above 500 MeV the acceptance at low p_T is good. This is illustrated in Figure 8. The general features of the acceptance for electron pairs are similar. In terms of the "transverse mass", $m_T = \sqrt{m^2 + p_T^2}$, the acceptance for electron pairs starts at $\sim 0.25\,\mathrm{GeV}$ and for muon pairs at around $\sim 0.4\,\mathrm{GeV}$.

As described in detail below, acceptance corrections are applied to the simulations of the various sources of lepton pairs used to describe the data.

4.2 Analysis of lepton pair mass spectrum

We shall now examine in detail various sources of lepton pairs, and the extent to which they can account for the data. After discussing the mass spectrum, we shall also consider the dependence on p_T, the event multiplicity, and atomic number of the target.

In the absence of any "new physics", the main sources of lepton pairs are expected to be hadronic decays. For electrons, π^0 Dalitz decay can be expected to dominate up to a pair mass of 140 MeV, whilst at higher mass the decays $\eta \to l^+l^-\gamma$ and $\omega \to l^+l^-\pi^0$ should be significant. For muons the 4m flight-path of the electron spectrometer results in a significant contribution from π and $K \to \mu\nu$ decays.

4.2.1 Contributions related to like-sign spectra

For di-muons the contribution from π and K decays can be estimated from the like-sign spectra. We define N^{+-} to be the number of $\mu^+\mu^-$ events from π and K decay, and similarly N^{++} and N^{--}. If the multiplicity of the parent hadrons is n^+ and n^- for positives and negatives respectively, then $N^{+-} \propto n^+n^-$, $N^{++} \propto n^+(n^+-1)$, $N^{--} \propto n^-(n^--1)$. This leads to:

$$N^{+-} = 2R\sqrt{N^{++}N^{--}}$$

where $R = \sqrt{n^+n^-/(n^+-1)(n^--1)}$, which evaluates to about 1.25 for our data, using average values for the multiplicities.

The above is over-simplified, and there are further effects due to the distribution of multiplicities, the differing π and K production spectra, and slightly different acceptances for like-sign and opposite-sign pairs. For any kinematic variable, e.g. the pair mass M, we define $R(M)$ by:

$$N^{+-}(M) = 2R(M)\sqrt{N^{++}(M)N^{--}(M)}$$

where $N^{+-}(M)$ is the number of events with $\mu^+\mu^-$ mass M from π and K decays etc. The overall effect of all factors (finite multiplicity, production spectra, acceptance, trigger, and reconstruction) has been studied by Monte Carlo, and leads to an $R(M)$ value of around 1.4 with some dependence on M.

The π and K decay contribution to the $\mu^+\mu^-$ mass spectrum is then formally given by $2R(M)\sqrt{N^{++}_{data}(M)N^{--}_{data}(M)}$. In practice, the like-sign spectra are somewhat limited in statistics, and a "mixed" event spectrum was used, i.e. μ^+ from one event and μ^-

from another, which offers very good statistical precision. Trigger conditions and relative acceptances were then applied to ensure that this mixed event spectrum was a true representation in both shape and normalisation of $\sqrt{N^{++}_{data}(M)N^{--}_{data}(M)}$.

The π and K contribution to the opposite-sign di-muon mass spectrum is shown in Figure 9b, labelled *"hadrons"*. It is around 50% over most of the mass region, except near threshold and in the ρ/ω and φ resonance regions. It should be noted that this estimate based on the like-sign spectra does *not* include "correlated" contributions like $\rho \to \pi^+\pi^- \to \mu^+\mu^-$, which gives a broad peak at $m_{\mu\mu} \sim 600\,\mathrm{MeV}$. These are estimated as described below.

The e^+e^- mass spectrum is not of course fed by π and K decays in the same fashion, though there is a small contribution of the same type from the $K \to \pi e\nu$ decay mode. The like-sign spectra are presumably dominated by e^+e^+ and e^-e^- pairs from two photon conversions. This effect will also contribute to the opposite-sign spectrum, and we have estimated it by $N^{++}+N^{--}$. This contribution to the e^+e^- spectrum is much less significant than for the muons, and it is subtracted in all subsequent plots.

We turn now to the contribution from decays of hadrons.

4.2.2 Contribution from decays of hadrons

The major contributions to the l^+l^- spectrum are expected to come from the decays in Table 2 as well as $c \to l^+; \bar{c} \to l^-$ (associated charm production).

reaction	production	decay
$\pi^0 \to e^+e^-\gamma$	B-G	K-W.form-factor
$\eta \to l^+l^-\gamma$	B-G	K-W.form-factor
$\rho/\omega \to l^+l^-$	B-G	$1+\cos^2\theta^*$
$\omega \to l^+l^-\pi^0$	B-G	K-W.form-factor
$\eta' \to l^+l^-\gamma$	B-G	K-W.form-factor
$\varphi \to l^+l^-$	B-G	$1+\cos^2\theta^*$

Table 2: Summary of production and decay mechanisms assumed for the principal hadronic decay contributions to l^+l^-. See text for discussion of the Bourquin-Gaillard (B-G) and Kroll-Wada (K-W) parametrisations, and the form-factors used.

In addition, for muons there is a significant contribution from the process: $\rho \to \pi^+\pi^- \to \mu^+\mu^-\nu_\mu\bar{\nu}_\mu$ which, as mentioned above, is not accounted for by the like-sign spectra. Smaller contributions of the same type arise from $\varphi \to K^+K^-$, $\varphi \to \rho\pi$, $\eta \to \pi^+\pi^-\pi^o$, and $\eta \to \pi^+\pi^-\gamma$, with subsequent decays of the π's and K's to muons.

The estimation of the above decay contributions requires a knowledge of the production and decay properties of all the relevant hadrons, combined with the detector acceptance. As discussed in more detail below, it is a crucial feature of our analysis that the normalisation of the most important contributions can be done using the data itself.

The production and decay properties we have assumed are summarised in Table 2. The Bourquin-Gaillard (B-G) parametrisation, [17], gives the parametric form of $d^2\sigma/dydp_T$ for the production in high-energy hadronic collisions of many different hadrons over the full phase-space. Since its appearance nearly 20 years ago, it has withstood rather well the advent of much new data. For the virtual photon decay into lepton pairs, we use the Kroll-Wada, [18], (K-W) expression[3)] multiplied by a form-factor. Branching ratios are taken from the 1992 Particle Data Book. Details for each of the particles are as follows:

$\pi^0 \to e^+e^-\gamma$: The B-G expression gives an excellent description of the data over the kinematic region of interest.

$\eta \to l^+l^-\gamma$: The K-W expression is multiplied by a Vector Dominance (VDM) form-factor. B-G gives an adequate description of recent data on η production from NA27 [20] and from our own experiment [21], but better fits can be devised over a restricted kinematic range. We have checked the sensitivity of our results to reasonable variation of the form of the production cross-section, and this is included in the systematic error.

For the decay, the VDM form-factor is supported by data from Lepton-G [22]. The helicity of the virtual photon is constrained to be ± 1.

$\rho/\omega \to l^+l^-$: We take the production cross-sections of ρ and ω to be equal, as measured by NA27 in 400 GeV/c pp collisions [20]. We find that B-G gives an excellent description of the y and p_T dependence of the dimuon data, as shown in Figure 10.

The decay-angle distribution of the di-leptons depends on the polarisation of the ρ/ω. Our data are limited to $\mid cos\theta^* \mid < 0.75$, and are consistent with the possibilities of a flat angular distribution and $1 \pm cos^2\theta^*$. We assumed $1 + cos^2\theta^*$, as observed in diffractive photo-production.

It is interesting to note that the branching ratio $\omega \to \mu^+\mu^-$ has never been measured; the Particle Data Group give an upper limit of 2.10^{-4} [24]. Our mass resolution in both $\mu^+\mu^-$ and e^+e^- pairs is substantially smaller than the ρ width, and a fit to the line shape in both $\mu^+\mu^-$ and e^+e^- requires a significant contribution of a resonance much narrower than the ρ. In other words, our data show direct evidence for $\omega \to e^+e^-$, which is well measured [25], and for $\omega \to \mu^+\mu^-$, which is not. The data also favour, slightly, coherent ("interfering") ρ/ω production with a phase of 2 radians, giving destructive interference. A publication on the determination of the branching ratio $\omega \to \mu^+\mu^-$ is in preparation [26].

The assumptions made about ρ/ω production and decay do not affect significantly the goodness of fit to the data, but only certain ratios of cross-sections which we infer from the data. This is discussed below.

$\omega \to l^+l^-\pi^0$: The production is as for the $\omega \to l^+l^-$. K-W is multiplied by the measured form factor for $\omega \to l^+l^-\pi^0$. There is only one measurement of this form-factor in the time-like region [27]. The data agree with the VDM for $m_{l^+l^-} < 0.5\,\mathrm{GeV}$, but exceed it by a factor of about 2 for the integrated form-factor above this mass, albeit with large errors. Such an effect obviously needs further experimental investigation; we have used the measured form-factor.

$\eta' \to l^+l^-\gamma$: K-W is multiplied by a VDM form-factor which is consistent with the limited data [28]. The form factor passes through the physical ρ/ω region which introduces some uncertainty. As for the η, the helicity of the virtual photon is constrained to be ± 1.

$\varphi \to l^+l^-$: Decay angular distribution as for the ρ/ω.

charm production: Charm production was generated using the Pythia Monte Carlo

[3] For the decay $A \to B\,l^+l^-$ the general expression is: (see for example [19]):

$$\frac{d\sigma}{dM} \propto \frac{1}{M}\left[1-\frac{4m_l^2}{M^2}\right]^{1/2}\left[1+\frac{2m_l^2}{M^2}\right]\left[\left(1+\frac{M^2}{m_A^2-m_B^2}\right)^2-\frac{4m_A^2M^2}{(m_A^2-m_B^2)^2}\right]^{3/2}$$

where m_A, m_B, m_l are the masses of A, B, and the lepton, and M is the mass of the l^+l^- system. This reduces to the usual expression for Dalitz decay when B is a photon.

[29], tuned to give the x and p_T distributions in accord with EHS data [30]. For the total charm cross-section we used our data on di-muon events with large missing energy, normalising to the φ [31]. The charm cross-section obtained in this way is somewhat larger than the EHS value (which corresponds to D production only), although consistent within errors.

The estimation of these hadronic contributions to the mass spectra proceeds by Monte-Carlo generation of production and decay, using the assumptions just described, followed by simulation of the detector response, trigger, and reconstruction. Because we always normalise to some feature seen in the data, (i.e. in effect all the results we obtain are ratios) imperfections in this simulation step tend to cancel out. There is one important exception, the photon reconstruction efficiency, for which an absolute value must be determined from Monte-Carlo, as described in the next section.

4.2.2.1 η Dalitz decay contribution

One of the merits of the HELIOS spectrometer is its ability to measure *all* the products of the Dalitz decay $\eta \rightarrow l^+l^-\gamma$, by combining the measurement of charged leptons with the measurement of photons seen in the electromagnetic section of the ULAC. In principle, the η Dalitz decay contribution to the di-lepton mass spectrum is then just those lepton pairs which combine with a photon to give the η mass. In practice, the situation is complicated by the photon reconstruction efficiency and background, as discussed further below. But the method still retains the great advantage that it is *independent* of the η production cross-section. Normalising the η contribution to another resonance (e.g. ρ/ω or φ) obviously introduces the experimental uncertainty in the cross-section ratio (η/resonance). The RISK collaboration has also used its own observation of the η Dalitz decay to normalize the η contribution to the mass spectrum. [32]

Photon showers are reconstructed as described in section 3.2. For the electron data, the photon candidate is required to be separated by at least 6cm from all other reconstructed showers. (The reason for the 6cm cut is explained below.) For the muon data less stringent photon reconstruction criteria are applied. The $e^+e^-\gamma$ and $\mu^+\mu^-\gamma$ data are shown as the solid points in Figure 11. A peak due to the η is clearly visible in both spectra, as is the π^0 in $e^+e^-\gamma$. For $\mu^+\mu^-\gamma$ the acceptance is poor for the η for $p_T(\mu^+\mu^-\gamma) < 750\,\mathrm{MeV/c}$.

To make quantitative use of this η signal, we must extract the number of η's seen in the $l^+l^-\gamma$ spectrum, and estimate the corresponding contribution to the l^+l^- mass spectrum. This latter step requires a knowledge of the relative acceptance of the detector for $l^+l^-\gamma$ compared to l^+l^-, and of the η production and decay. The production and decay enter because η's reconstructed in $l^+l^-\gamma$ cover a smaller region of phase space than the η Dalitz decays which feed the l^+l^- mass spectrum, for which only the l^+ and l^- are required to be reconstructed, and so an extrapolation is required. This is particularly relevant for muons because of the limited p_T acceptance for $\mu^+\mu^-\gamma$, and is reflected in the errors as discussed below. which the somewhat larger

The relative acceptance for $l^+l^-\gamma$ compared to l^+l^- is the photon reconstruction efficiency, which is determined as follows. The Monte-Carlo of the e.m. section of the ULAC is in excellent agreement with the energy response, resolution, and longitudinal and lateral shower profiles observed in real data. For the photon reconstruction efficiency in the di-muon case, single showers are generated over the required kinematic range, and superposed on to real di-muon events. These events are then processed through the standard analysis chain, and the photon reconstruction efficiency is inferred.

For e^+e^- we require the photon reconstruction efficiency for events in which (at

least) two other e.m. showers are also reconstructed. The photon reconstruction efficiency for such events has been determined by generating three showers (from η Dalitz decay) and superposing them on real di-muon data. (The reason for using di-*muon* events, rather than di-electron events, is that the former give the appropriate hadronic multiplicity and corresponding activity in the ULAC e.m. section. The latter have in addition (at least) two e.m showers, which would bias the estimation of the efficiency.) The events so obtained were then processed through the standard analysis chain, and the photon reconstruction efficiency extracted from events in which all three showers are reconstructed. The efficiency turned out to differ only slightly from the shower efficiency in single-shower events. The efficiency was checked using the π^o observed in e^+e^- and in $e^+e^-\gamma$. This check worked well with the requirement of at least 6cm between shower centres, and less well at 4cm, which is reason for the 6cm cut.

The η peak seen in the $l^+l^-\gamma$ data, Figure 11, sits on substantial combinatorial background. We use a "mixed event" spectrum (l^+l^- from one event, photon from another) to determine the shape of this background. Apart from this background and the η itself, there are other decays which could contribute significantly: $\pi^0 \to e^+e^-\gamma$ (seen clearly in the data), $\eta' \to l^+l^-\gamma$, and $\omega \to l^+l^-\pi^0$, where one of the photons from the π^0 decay is missed. The π^0, η, ω, and η' are generated with the production and decay characteristics as given in section 4.2.2, and then passed through the simulation of the detector, trigger, and reconstruction. The relative production cross-sections of π^0, η, and ω are taken from [20]. The η'/π^0 cross-section is estimated using the measured η'/π^0 ratio at high p_T [33] and the B-G parametrisation.

The fit to the $l^+l^-\gamma$ spectrum requires one overall normalisation factor for the hadronic decay contributions and another for the combinatorial background. The various contributions are shown separately in Figure 11 together with the overall fit. The high mass "tail" on the π^0 is an artefact of the requirement of spatial separation between the three e.m. showers in the calorimeter. Contributions from the ω and η' at the expected levels are favoured by the data, but not with great statistical significance. [4)]

The Monte-Carlo normalisation factor which fits the $l^+l^-\gamma$ spectrum also fixes the prediction of the η Dalitz decay contribution to the l^+l^- spectrum.

This η contribution to the mass spectra is shown in Figure 9b for muons, and in Figure 12b for electrons. The error in the estimated contribution is 25% in each case. However, the significant sources of error are different in the two cases: for electrons the efficiency for finding three e.m. showers required evaluation, whilst for muons the kinematic extrapolation in p_T is larger.

It should be noted that imperfections in the simulation which affect both the l^+l^- and $l^+l^-\gamma$ channels cancel out in the determination of the η Dalitz contribution; only the photon finding efficiency and the extrapolation from the $l^+l^-\gamma$ kinematic region to the l^+l^- kinematic region enter in an absolute way.

It can be seen that the η Dalitz decay accounts for almost all electron pairs from 0.16 GeV up to ~ 0.4 GeV, and, together with the π and K decay contribution, for the majority of muons from threshold up to ~ 0.4 GeV.

The procedure for estimating the η Dalitz decay contribution has been described in detail. The principle is used for all contributions: select an appropriate feature seen

[4)] Since the form-factor we have used for the $\omega \to l^+l^-\pi^0$ decay is controversial, we have studied the contribution of $\omega \to e^+e^-\pi^0 \to e^+e^-\gamma$ with one γ missed to the $e^+e^-\gamma$ spectrum, for different values of $m_{e^+e^-}$. Our data are consistent with the form factor measured by Lepton-G at large values of $m_{e^+e^-}$, but are far from being statistically decisive.

directly in the data, and use it to normalise the Monte-Carlo predictions.

4.2.2.2 $\omega \rightarrow l^+l^-\pi^0$ contribution

The decays $\omega \rightarrow e^+e^-\pi^0$ and $\mu^+\mu^-\pi^0$ have both been measured [34] [27], and can be expected to contribute significantly to the di-lepton mass spectrum. As discussed in the previous section, our $l^+l^-\gamma$ spectra (see Figure 11) allow a contribution at the expected level from this decay mode, where one photon from the π^0 is missed, but the statistical significance is too weak to be able to use it for normalisation. Instead, for electrons we use the ρ/ω signal seen in e^+e^- and for muons the φ seen in $\mu^+\mu^-$. The use of the φ for muons brings in the uncertainty in the relative ω to φ production cross-sections, but avoids the more complicated ρ/ω region. For electrons the φ is statistically weak, and in any case the resonance to background ratio in the ρ/ω region is better.

We now proceed exactly as for the η Dalitz decay, by generating the sources according to the assumptions described in sect. 4.2.2, followed by the trigger, detector, and reconstruction simulations. Normalisation to the ρ/ω and φ seen in the data then determines the contribution of $\omega \rightarrow l^+l^-\pi^0$ decay to the l^+l^- mass spectrum. This contribution is shown in Figure 9b for muons, and in Figure 12b for electrons. The error on this contribution is around 35% for electrons and about 45% for muons.

The η Dalitz decay and $\omega \rightarrow e^+e^-\pi^0$ contributions are sufficient to explain all the e^+e^- spectrum up to $\sim$ 0.6 GeV, and, together with the π and K decay contribution, almost all the $\mu^+\mu^-$ spectrum up to around 0.5 GeV.

For the muons the ρ/ω is an alternative normalisation and leads to a $\omega \rightarrow \mu^+\mu^-\pi^0$ contribution consistent with that obtained using the φ, and with roughly comparable error.

Having simulated η, ρ, and ω production, we can infer the value of $\sigma_\eta/\sigma_{\rho/\omega}$ required by our data. We obtain 0.54 ± 0.05 from the electron data and 0.52 ± 0.06 from the muons. The assumption made about ρ/ω interference affects this ratio: the interference phase we have used gives a negative contribution, i.e. the quantity $\sigma_{\rho/\omega}$ is less than the sum of the production cross-sections $\sigma_\rho + \sigma_\omega$. So in order to compare our ratio to the quantity $\sigma_\eta/(\sigma_\rho + \sigma_\omega)$, as measured for example by NA27 [20], we must correct for the interference effect. This leads to a 15% reduction in our ratios to 0.46 ± 0.04 and 0.44 ± 0.05 for electrons and muons respectively. The NA27 result is 0.385 ± 0.033.

Most previous analyses of low-mass lepton pair production have used an η cross-section measured in other experiments. This can bring in large uncertainties. For example, it is now clear that the value of 0.17 for $\sigma_\eta/(\sigma_\rho+\sigma_\omega)$, based on an extrapolation of exclusive channels measured in πp and Kp collisions at 10 and 16 GeV/c [35], is an under-estimate of the η contribution in high-energy proton collisions.

We stress again that our own estimation of the η contribution to the l^+l^- mass spectrum in no way relies on the η to ρ/ω ratio, but is obtained by normalising to the η seen in $l^+l^-\gamma$. The η to ρ/ω ratio is merely a by-product of our fits. Indeed, our value for the ratio is also sensitive to the assumption of the polarisation of the ρ and ω. We have assumed that they are produced polarised so as to give a $1 + cos^2\theta$ distribution. If instead they are produced unpolarised, as suggested by some data [23], our value for $\sigma_\eta/(\sigma_\rho + \sigma_\omega)$ will increase by about 20%.

4.2.2.3 Other contributions to the mass spectrum

Several other contributions to the mass spectrum have been estimated in similar fashion, and are shown in Figures 9 and 12.

For electrons the π^0 Dalitz contribution is estimated by normalising to the ρ/ω, or to the π^0 seen directly in $l^+l^-\gamma$. The two methods agree. This checks our understanding of trigger efficiency and acceptance over the e^+e^- mass range from 50 MeV up to the ρ.

For muons, it is interesting to note that the data seem to require a contribution of $\eta \rightarrow \mu^+\mu^-$. [5] Normalising to the φ, we can infer the branching ratio for $\eta \rightarrow \mu^+\mu^-$ required to fit our data, and find $2.6 \pm 1.1\,10^{-5}$. This is higher by a factor of 4 than the recent measurement by Saturne II [36], but our error is much larger.

For muons and electrons, the charm contribution turns out to be insignificant in the low-mass region.

Apart from hadronic decays, there are two other processes which could contribute:

- The Drell-Yan process is the dominant source of lepton pairs in the high-mass (> 2 GeV) continuum. It is not clear how to calculate a Drell-Yan-like contribution at low mass ($< m_\rho$), and we have made no attempt to do so. In any case our data do not require any substantial contribution.
- Bremsstrahlung of virtual photons is expected to be a significant contribution to the pair spectrum at very low mass, and in particular at very low transverse mass. However, there are difficulties in calculating this contribution. [37] We have made an estimate of the contribution to the muon-pair spectrum, summing the contributions from each final state hadron "incoherently", using the PYTHIA Monte-Carlo to generate the hadrons, and normalising to the φ seen in the data. This contribution is shown in Figure 9. However, it is almost certainly a substantial over-estimate, and is presented as indicative only.

The overall result is that the di-lepton mass spectrum is explained entirely satisfactorily by conventional sources. We comment in more detail in section 5. A reasonable way of summarising the result is that in high-energy p-Be collisions the mass spectrum below the ρ of centrally produced di-leptons is accounted for largely by η and ω decays with $\sigma_\eta/(\sigma_\rho + \sigma_\omega)$ around 0.4-0.5, and production in accord with the Bourquin-Gaillard parametrisation.

4.2.3 p_T dependence

We have investigated the p_T dependence of the data by studying the mass spectra for p_T of the lepton pair < 800 MeV/c and $p_T > 800$ MeV/c. The results are shown in Figures 13.

As for the mass spectrum integrated over all p_T, it is seen that known sources account for the data rather satisfactorily. The muon data show an excess over the estimated sources in the mass region between the ρ and the φ for $p_T < 800$ MeV/c, Figure 13b. For electrons, the high p_T data suggest an excess in the mass range $0.4 - 0.6$ MeV, Figure 13c.

We have also looked at the data as a function of p_T, rather than mass, as shown in Figures 14. Once again, known sources describe the spectra. For muons the data have also been analysed in terms of the di-lepton rapidity, and are well described by the same mixture of sources [15].

4.2.4 Multiplicity dependence

The dependence of lepton pair production on the hadronic multiplicity has been suggested as a useful way of discriminating among different production mechanisms [38]. The essential point is that if a lepton pair is produced as a decay product of a single

[5] The decay $\eta \rightarrow e^+e^-$ is suppressed relative to $\mu^+\mu^-$ by $(m_e/m_\mu)^2$.

hadron, then the rate of lepton pair production should depend *linearly* on the hadronic multiplicity. On the other hand, if each lepton of the pair comes from a separate hadron, or if the pair is produced by a process like annihilation between *final* state quarks and anti-quarks, then the rate of lepton pair production should depend *quadratically* on the hadronic multiplicity.[6] There are also mechanisms, like Drell-Yan, which are expected to be independent of the multiplicity.

Hence it is interesting to examine the multiplicity dependence of di-lepton production. For the $\mu^+\mu^-$ data, where we have higher statistics than in e^+e^-, we define the quantity:

$$H = n_{ch}.(\text{“}\mu^+\mu^-\text{”} - \text{“}\pi/K\text{”})/\text{“}\pi/K\text{”}$$

where n_{ch} is the raw charged multiplicity, including the two muons, as determined from the Si pad detector, “$\mu^+\mu^-$” is the number of $\mu^+\mu^-$ events with multiplicity n_{ch}, and “π/K” is the number of such events from π and K decay. This last number is estimated by $2R\sqrt{N^{++}N^{--}}$, where R is a function of multiplicity, as discussed in section 4.2.1. The quantity H is constructed so that if (“$\mu^+\mu^-$” − “π/K”) depends linearly on n_{ch}, and if (“π/K”) depends quadratically as it should, then H will be a constant independent of the multiplicity. However, for a signal like the ρ, fits to bubble-chamber data [39] suggest a dependence like $(n_{ch} - 2)$, where n_{ch} is the total charged multiplicity in the event. If this dependence applied in our case, H would behave as $(n_{ch} - 2)/n_{ch}$.

As our estimate for the total charged multiplicity is crude, we focus on the comparison of H as a function of multiplicity for different mass regions. The data for four different mass regions are shown in Figure 15. The ρ/ω region is consistent with a linear dependence on n_{ch}, but $(n_{ch} - 2)$ is not strongly excluded. In any case, there is nothing to suggest any striking difference between the behaviour in the ρ/ω region and that in the lower mass bins. In the φ mass region there is a suggestion that H rises linearly, implying a quadratic dependence for the φ itself. Such an effect would be puzzling. Our data are more than a 3σ effect, but we note again that H might behave as $(n_{ch} - 2)/n_{ch}$, as well as the possibility that the φ might be produced with extra charged kaons, which would give a behaviour similar to that observed. Further investigation is needed.

In summary, the two mass bands below the ρ/ω are consistent with having the same multiplicity dependence as the ρ/ω, although the statistics preclude a very strong conclusion.

4.2.5 Target A dependence

Spurred by the interest in di-lepton production in ultra-relativistic heavy-ion collisions and by other theoretical speculations [40], we carried out a limited study of the dependence of lepton pair production on the atomic number of the target. The Be target was replaced by an Ag target of length 1 cm ($\sim 1X_0$) and diameter 50 μm for a short running period at the end of the main data-taking. Whilst statistics were limited, the aim was to check for any dramatic A-dependence in the di-lepton yield. We present here results on a comparison of e^+e^- production in p-Be and p-Ag collisions.

The data-taking and triggering were exactly as described in section 2. The electron reconstruction differed in minor details to that described in section 3.2, but for the purposes of the Be/Ag comparison a sample of the Be data and the Ag data were processed in *identical* fashion.

[6] Assuming that the number of final state quarks (or anti-quarks) is proportional to the hadronic multiplicity.

The overall characteristics of the events with the two targets are similar, though the mean charged multiplicity (as recorded by the Si-pad detector) is 10.2 for Ag and 8.2 for Be, and the energy per particle is somewhat lower for Ag.

The Ag data yielded 208 events of which 136 were e^+e^- and 72 were e^+e^+ or e^-e^-. The Be sample gave 1444 events of which 1214 were e^+e^- and 230 were e^+e^+ or e^-e^-. The dependence of the efficiency of the event reconstruction on event multiplicity and particle energy has been studied, with the result that the Ag yield must be multiplied by 2.0 ± 0.6 to compare to the Be yield. This gives:

$$e^+e^-_{Ag}/e^+e^-_{Be} = 1.7 \pm 0.4(stat.) \pm 0.8(syst.)$$

where $e^+e^-_A$ is the e^+e^- yield per charged particle for the particular target, and the systematic error includes the uncertainty in the relative efficiency correction mentioned above, and an estimate of the dependence on the selection cuts.

The purpose of the measurement was to check for any large effect in going from a Be to a Ag target. Our result excludes such an effect.

5 Results and Conclusions

We have studied the central production of low mass electron pairs and muon pairs in hadronic collisions.

The strengths of our experimental approach are:

- The normalisation of hadronic sources is set by the data, through the direct observation of various hadronic resonances;
- We have carried out two essentially independent measurements in electron pairs and muon pairs, which emphasise different aspects of the detector, and have quite different backgrounds.

The results are:

- Both electron pairs and muon pairs can be explained entirely satisfactorily by pairs produced by hadronic decays, and there is no need to invoke any other low-mass source. The mass spectrum between 140 MeV and the ρ/ω is accounted for largely by η and ω decays with $\sigma_\eta/(\sigma_\rho + \sigma_\omega)$ around 0.4-0.5, and production in accord with the Bourquin-Gaillard parametrisation.
- The explanation in terms of hadronic decays holds whether the data are analysed in terms of the mass or of the p_T of the pair. (See Figures 9, 12, and 14.)
- The upper limits at 90% confidence level on any other source of lepton pairs are given in the following table, as a percentage of the hadronic decay contribution:

Mass (MeV)	140-200	200-260	300-360	400-460
e^+e^-	29%	37%	48%	39%
$\mu^+\mu^-$		21%	20%	20%

- Results on the multiplicity dependence and the target A dependence support, within the limited statistics, the conclusion that the pairs come from conventional sources.

Two points arising from our analysis are worth noting:

- As we have stressed, several previous analyses have suffered from uncertainty about the η Dalitz contribution. We avoid this uncertainty by direct observation of the Dalitz decay. As a by-product, we obtain a value of between 0.4 and 0.5 for $\sigma_\eta/(\sigma_\rho + \sigma_\omega)$, depending on what we assume in detail for the ρ/ω production, in reasonable agreement with [20]. This value is substantially larger than what might have been inferred from results at low energy.

- Although the η problem is resolved, there remains an uncertainty associated with the high mass part of the $\omega \rightarrow l^+l^-\pi^0$ form-factor. Our data are not adequate to check the form-factor directly, but it may be noted that the e^+e^- data favour the ω contribution with a large form-factor in the mass region 0.5 to 0.6 GeV. This can be seen in Figure 12b, where the mass region 0.5 to 0.6 GeV is dominated by this contribution. On the other hand, in muon pairs there are some other contributions in this mass region, and the data if anything disfavour a large form-factor. This is best seen in Figure 9a, where the data are on the low edge of the prediction for this mass range. A decisive experiment on the ω form-factor is needed.

In comparing our results to those of previous experiments, we make the following observations:

- Most claims of an excess of low-mass pairs are sensitive to the level of η production assumed. It is now clear that the high energy experiments in general assumed too low a value. (In the significantly different kinematic regime of pair p_T (> 2 GeV/c), an ISR experiment [41] saw an "excess" in the $0.4 - 0.6$ GeV mass region, which can be attributed to charm.)
- Some of the authors of the present paper were also authors of two papers on single positron production at low p_T at the CERN ISR [42], which reached conclusions rather different in spirit to those presented here. The ISR experiment measured single positrons, with the requirement that the mass of the positron and any negative particle be greater than 100 MeV. A signal over and above all known sources was claimed, and furthermore this signal appeared to depend quadratically on the hadronic multiplicity. Neither result was statistically overwhelmingly strong, but they were certainly suggestive. It should be noted that the conclusion was not due to the use of too small a value of η production: η production was measured in the same experiment [43]. It is of course possible that the difference is due to the different $\sqrt{s}$ values.
  We have also measured single-electron production in the present experiment, using a different configuration of the detector. The data cuts were such that the mass of the parent pair was peaked below 100 MeV, and hence the sensitivity was different to that of the ISR experiment. Preliminary results have been reported [44], and suggest no unexpected behaviour in signal size or multiplicity dependence. A publication is in preparation.

Provided any new source is in lepton pairs rather than single leptons, it is of course much better to study pairs directly, as done in the analysis reported here. The present experiment is also superior by virtue of measuring both electrons and muons, and in its use of internal normalisation. It seems that there are no "unconventional" sources of low mass lepton pairs at a level comparable to the conventional sources.

6 Acknowledgements

The HELIOS collaboration wishes to thank the staff of the PS-SPS accelerator complex for their excellent work in providing the high quality proton beam used in this experiment. The valuable contributions of the technical staff of CERN and the collaborating institutes are gratefully acknowledged. We also wish to acknowledge the support received from the various research councils and funding agencies in our home countries.

References

[1] e^+e^- pairs:
J. Ballam et al. Phys. Rev. Lett. **41** (1978) 1207;
J.H. Cobb et al. Phys. Lett. **78B** (1978) 519;
A. Chilingarov et al. Nucl. Phys. **B151** (1979) 29;
R. Stroynowski et al. Phys. Lett. **97B** (1980) 315;
S. Mikamo et al. Phys. Lett. **106B** (1981) 428;
A.T. Goshaw et al. Phys. Rev. **D24** (1981) 2829;
J. Stekas et al. Phys. Rev. Lett. **47** (1981) 1686;
D. Blockus et al. Nucl. Phys. **B201** (1982) 205;
M.R. Adams et al. Phys. Rev. **D27** (1983) 1977;
V. Hedberg, PhD thesis, Univ. of Lund, LUNFD6/(NFFL-703)/1987, (1987)
G. Roche et al. Phys. Rev. Lett. **61** (1988) 1069;
C. Naudet et al. Phys. Rev. Lett. **62** (1989) 2652;
H.Z. Huang et al. LBL Preprint 32808 (1992)
$\mu^+\mu^-$ pairs:
K.J. Anderson et al. Phys. Rev. Lett. **37** (1976) 799;
J.G. Branson et al. Phys. Rev. Lett. **38** (1977) 1334;
G.G. Henry, PhD thesis, Enrico Fermi Inst., Univ. Chicago (1978);
H. Kasha et al. Phys. Rev. Lett. **36** (1976) 1007;
K. Bunnell et al. Phys. Rev. Lett. **40** (1978) 136;
B. Haber et al. Phys Rev. **D22** (1980) 2107;
J. Alspector et al. Phys. Lett. **81B** (1979) 397;
W.M. Morse et al. Phys. Rev. **D18** (1978) 3145;
R.I. Dzhelyadin et al. Nucl. Phys. **B179** (1981) 189;
M. Faessler et al. Phys. Rev. **D17** (1978) 689;
D.M. Grannan et al. Phys. Rev. **D18** (1978) 3150;
A.V. Bannikov et al. Proceedings of the Pittsburgh Workshop on Soft Lepton Pair and Photon Production, Ed. Julia A. Thompson (Nova Science Publishers Inc., 1992), pp. 163-173.
Significant results on *single* electrons or positrons include:
L. Baum et al. Phys. Lett. **B60** (1976) 485;
A. Browman et al. Phys. Rev. Lett. **37** (1976) 246;
E.W. Beier et al. Phys. Rev. Lett. **37** (1976) 1117;
M. Barone et al. Nucl. Phys. **B132** (1978) 29;
Y. Makdisi et al. Phys. Rev. Lett. **41** (1978) 367;
R. Barloutaud et al. Nucl. Phys. **B172** (1980) 25;
A. Maki et al. Phys. Lett. **B106** (1981) 423;
T.Åkesson et al. Phys. Lett. **152B** (1985) 411;
T.Åkesson et al. Phys. Lett. **192B** (1987) 463

[2] L. Van Hove, Ann. Phys. **192** (1989) 66

[3] For a recent review see P.V. Ruuskanen JYFL-18-92 (1992); to appear in "Particle Production in Highly Excited Matter", editor H.H. Gutbrod.

[4] R.H. Beuttenmuller et al. NIM **A252** (1986) 471

[5] R.H. Beuttenmuller et al. NIM **A253** (1987) 500

[6] K.H. Dederichs, PhD Thesis, Chapter 3, Ludwig-Maximilians-Universität (1989)

[7] T.Åkesson et al. NIM **A262** (1987) 243

[8] B. Dolgoshein NIM **A326** (1993) 434; in particular section 5.1.3

[9] M.J. Clemen, University of Pittsburgh Thesis (1989) and Y.M. Park, University of Pittsburgh Thesis (1990).
[10] C.W. Fabjan et al. Paper 775 submitted to XXIV International Conference, Munich 1988; HELIOS Note 174 (1986); SSC Detector R&D at BNL, Editors Yu and Radeka, BNL 52244, (1990), 14
[11] J. Badier at al. NIM **A175** (1980) 319
[12] R. Hammarstrom et al. NIM **A176** (1980) 137
[13] M. Morpurgo, Cryogenics **19** (1979) 411
[14] F. Gibrat, Université Paris 6 Thesis, CEA-N-2611 (1989)
[15] R.J. Veenhof, Universiteit van Amsterdam Thesis, (1993)
[16] C.W. Fabjan et al. NIM **A216** (1983) 105
[17] M. Bourquin and J-M Gaillard Phys. Lett. **59B** (1975) 191 and Nucl. Phys. **B114** (1976) 334.
[18] N. Kroll and W. Wada Phys. Rev. **98** (1955) 1355
[19] L.G. Landsberg, Phys. Rep. **128** (1985) 301, section 3.1
[20] M. Aguilar-Benitez et al. Z. Phys. **C50** (1991) 405
[21] HELIOS/1 $\eta \to \gamma\gamma$ in preparation.
[22] R.I. Dzhelyadin et al. Phys. Lett. **94B** (1980) 548
[23] J.G. Branson et al. Phys. Rev. Lett. **38** (1977) 1331
[24] The $\omega \to \mu^+\mu^-$ upper limit is a private communication to the Particle Data Group.
[25] See Particle Data Group review.
[26] HELIOS/1 $\omega \to \mu^+\mu^-$ in preparation. See also S. Johansson, University of Lund Thesis, LUNFD6/(NFFL-7057)/1-142(1990) and R.J. Veenhof, Universiteit van Amsterdam Thesis, (1993)
[27] R.I. Dzhelyadin et al. Phys. Lett. **102B** (1981) 296
[28] V.A. Viktorov et al. Sov. J. Nucl. Phys. **32** (1980) 520
[29] H.U. Bengtsson and T. Sjöstrand Pythia 5.3, CERN Program Library W5045
[30] M. Aguilar-Benitez et al. Phys. Lett. **B189** (1987) 476, and Z. Phys. C. **40** (1988) 321
[31] P. Aubry, University of Montreal Thesis, (1994) and P. Pomianowski, University of Pittsburgh Thesis, (1994). Also HELIOS/1 $e\mu$ and $\mu\mu$ events with missing energy: in preparation.
[32] A.V. Bannikov et al. Proceedings of the Pittsburgh Workshop on Soft Lepton Pair and Photon Production, Ed. Julia A. Thompson (Nova Science Publishers Inc., 1992), pp. 163-173.
[33] M. Diakanou et al. Phys. Lett. **89B** (1980) 432
[34] S.I. Dolinsky et al. Yadernaya Fisika **48** (1988) 442
[35] J. Bartke et al. Nucl. Phys. **B118** (1977) 360
[36] R.S. Kessler et al. Phys. Rev. Lett. **70** (1993) 892
[37] P. Lichard, SUNY-NTG-94-16 (1994). We also acknowledge useful discussions with P.Lichard and J.Pišút on hadronic bremsstrahlung.
[38] V. Černý et al. Z. Phys. C **31** (1986) 163 and P. Lichard in Proceedings of the Pittsburgh Workshop on Soft Lepton Pair and Photon Production, Ed. Julia A. Thompson (Nova Science Publishers Inc., 1992), p. 61.
[39] For example:
R. Singer et al. Phys. Lett. **60B** (1976) 385;
P.D. Higgins et al. Phys. Rev. **D19** (1979) 65;
M. Schouten et al. Z. Phys. C **9** (1981) 93

[40] P. Lichard, Z. Phys. C **37** (1987) 125
[41] A. Chilingarov et al. Nucl. Phys. **B151** (1979) 29
[42] T.Åkesson et al. Phys. Lett. **152B** (1985) 411 and T.Åkesson et al. Phys. Lett. **192B** (1987) 463
[43] T.Åkesson et al. Phys. Lett. **178B** (1986) 447
[44] J.A. Thompson et al. Hadron Structure 1991, p.126, ed. L. Martinovic, Bratislava, 1991

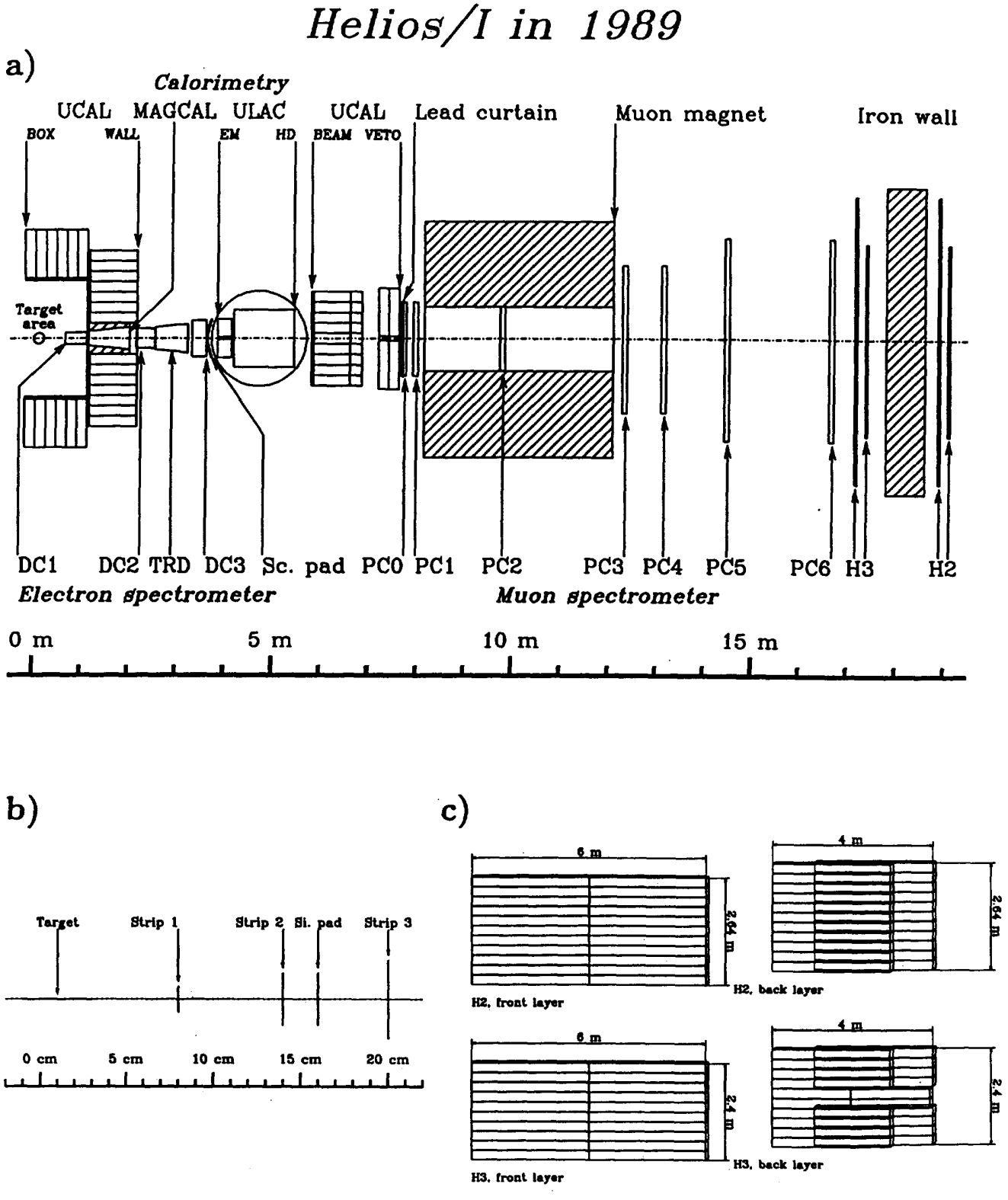

Figure 1: a) Overview of HELIOS detector for 1989 run, showing the major components. b) Blow-up of Target region. c) Front view of H3 and H2 muon trigger hodoscopes.

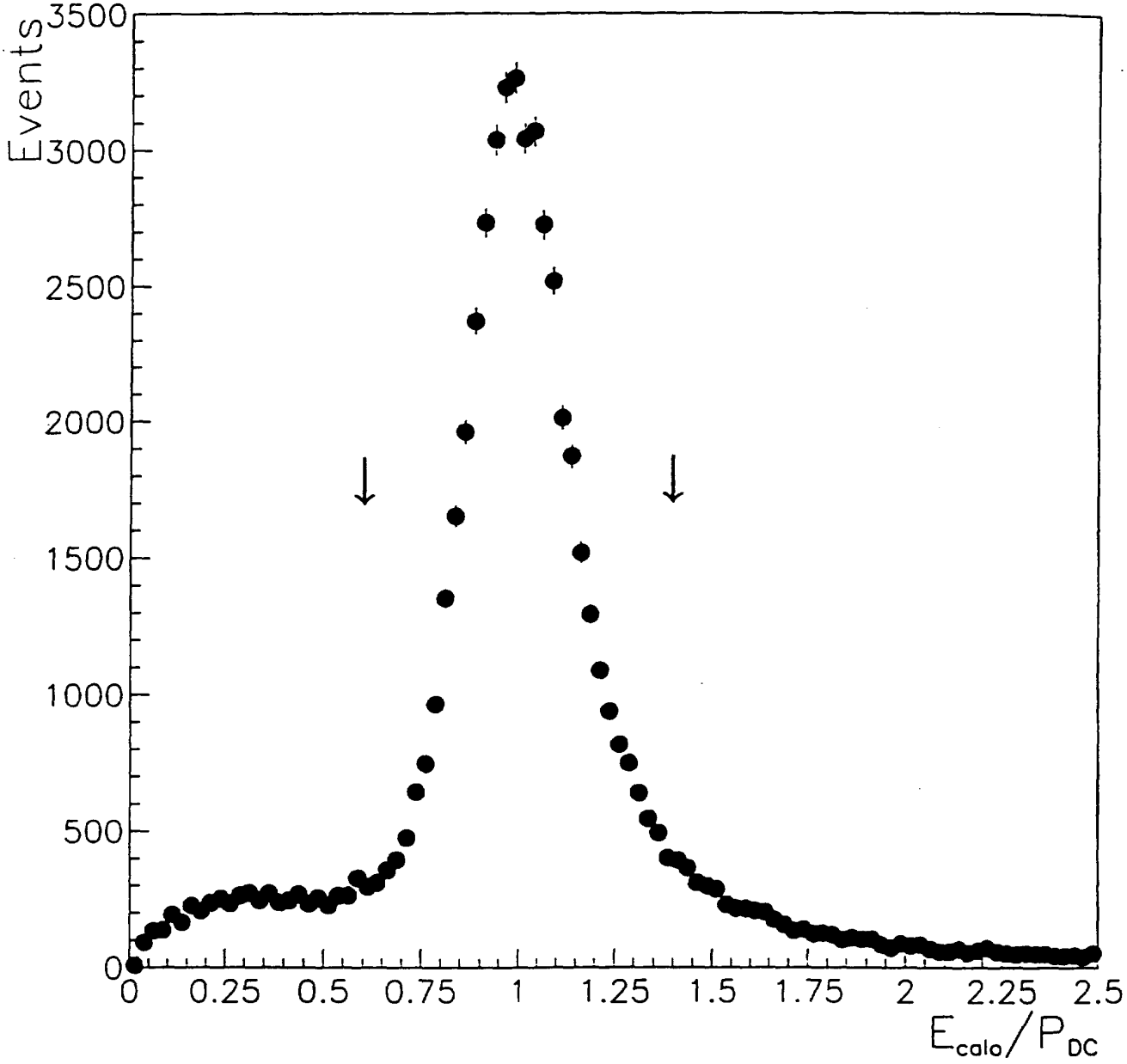

Figure 2: Ratio of ULAC shower energy (E_{calo}) to Drift Chamber momentum (P_{DC}) for electron track candidates, after matching of Drift Chamber track to shower position to within 1cm, and application of off-line trigger checks. The selection cuts are indicated by vertical arrows.

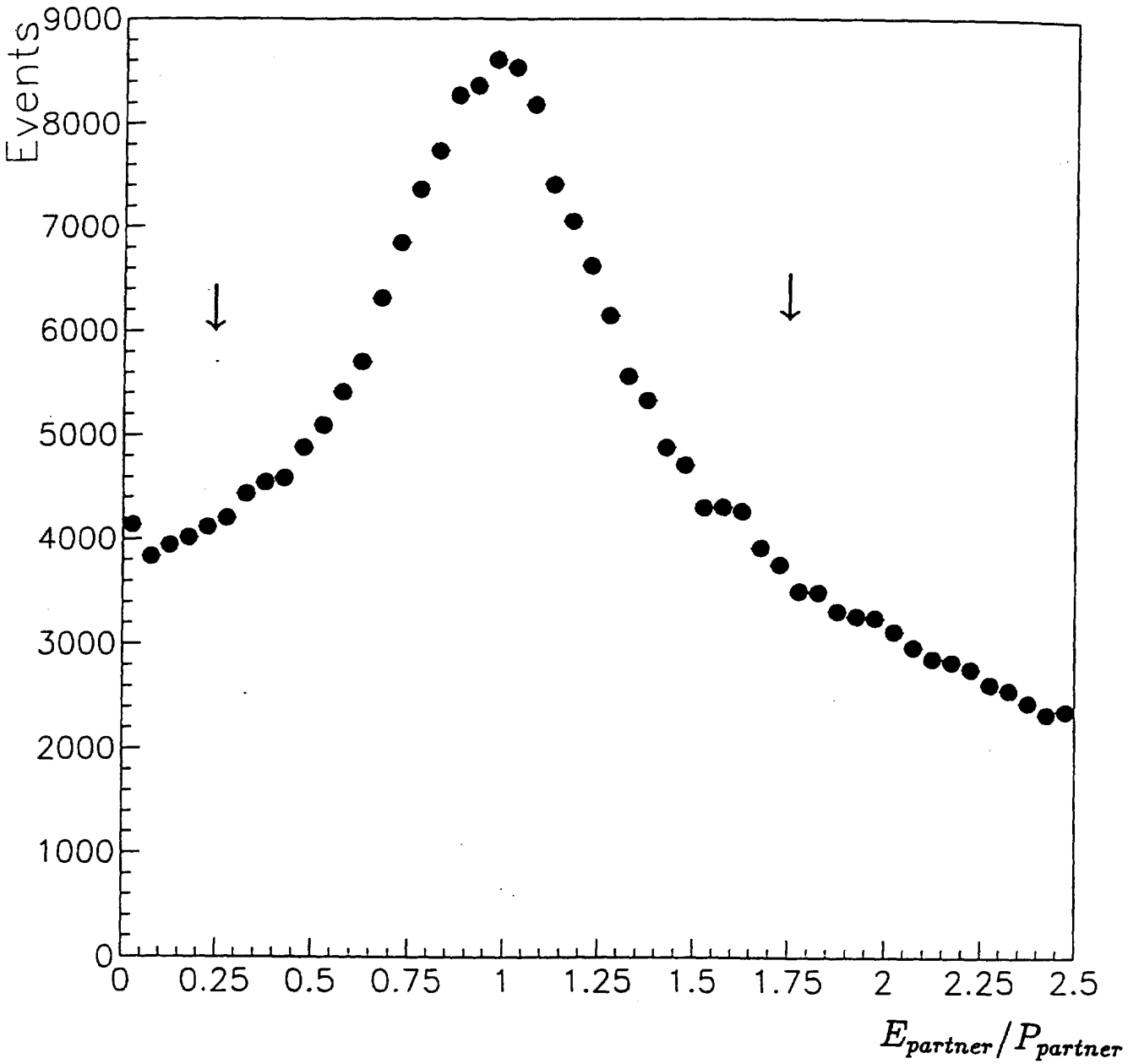

Figure 3: The ratio of $E_{partner}$ to $P_{partner}$, as explained in the text. The broad peak around 1 indicates the presence of conversion partners missed by the Drift Chamber reconstruction. The selection cuts are indicated by vertical arrows.

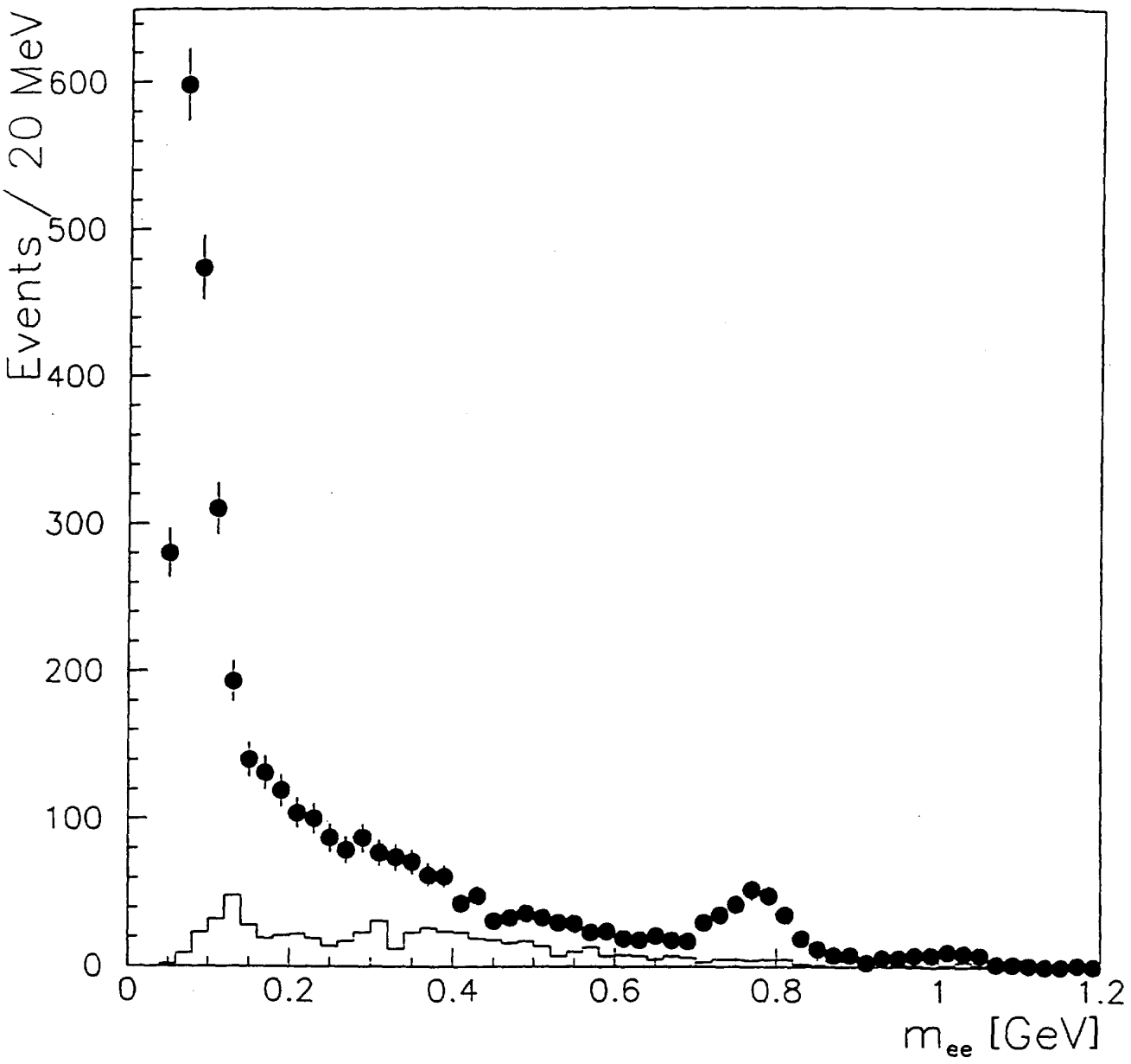

Figure 4: Mass spectrum of final sample of di-electron events. Full circles: e^+e^-; Solid histogram : sum of e^+e^+ and e^-e^-.

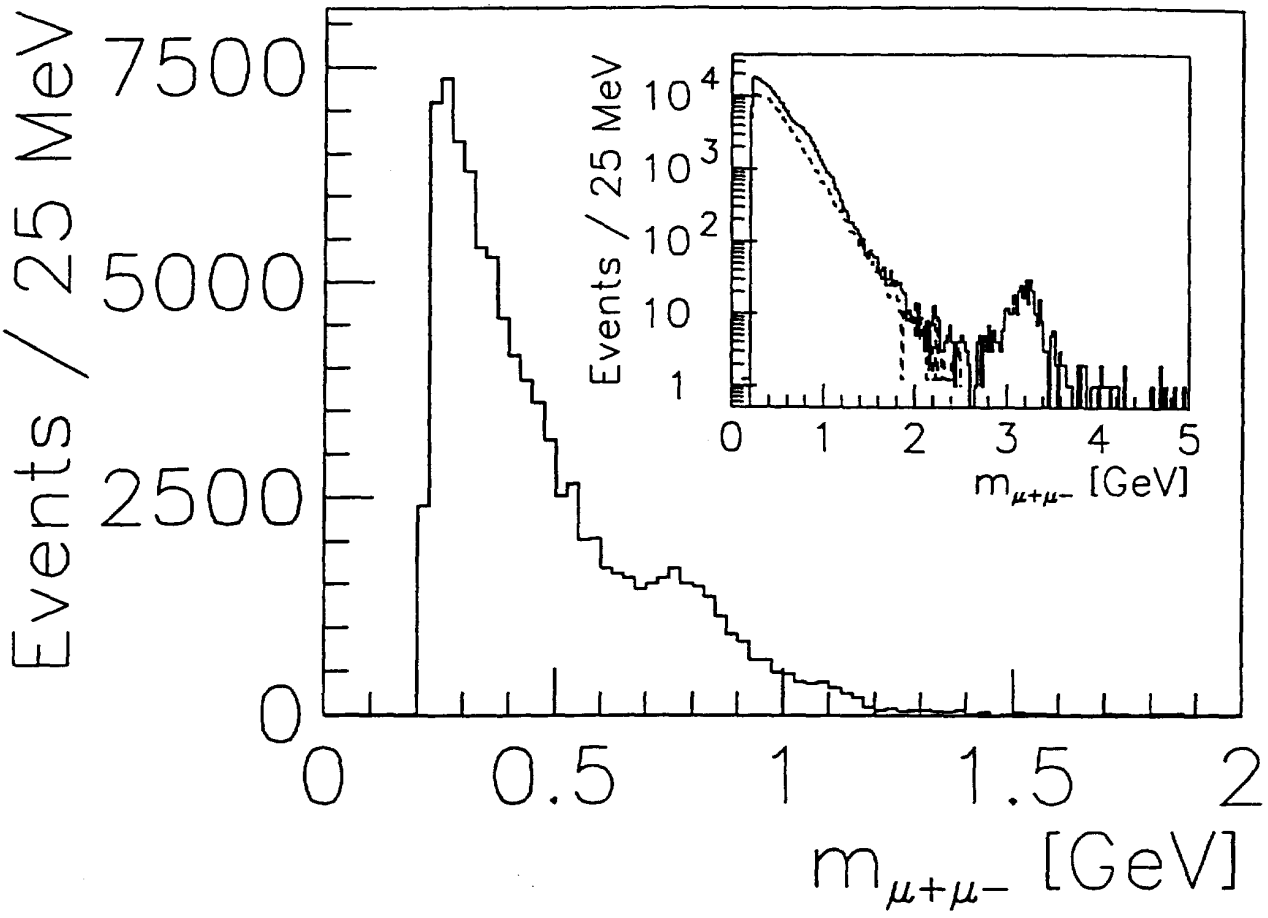

Figure 5: Like-sign subtracted mass spectrum of a sample of di-muon events after off-line reconstruction in the muon spectrometer only; i.e. no use has been made of track information in the upstream electron spectrometer. The inset shows the unsubtracted mass spectrum on a log scale to show the J/ψ.

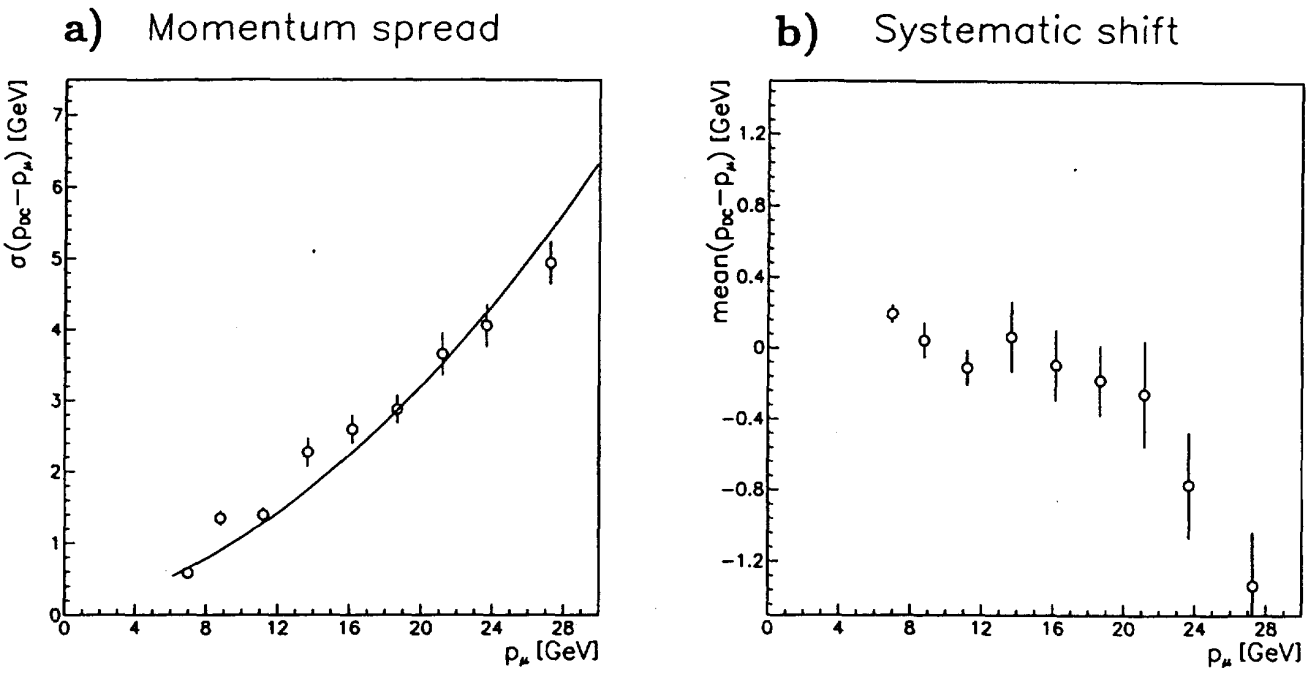

Figure 6: a) The r.m.s of $p_\mu - p_{DC}$ versus p_μ. The DC resolution (solid line) is sufficient to explain the data. Hence any fluctuation in the muon energy loss in the calorimeters is small.
b) The mean value of $p_\mu - p_{DC}$ versus p_μ. The systematic deviation is also seen in data taken with the calorimeters removed [15]. Hence the energy loss of the muon in the calorimeter is being estimated correctly.

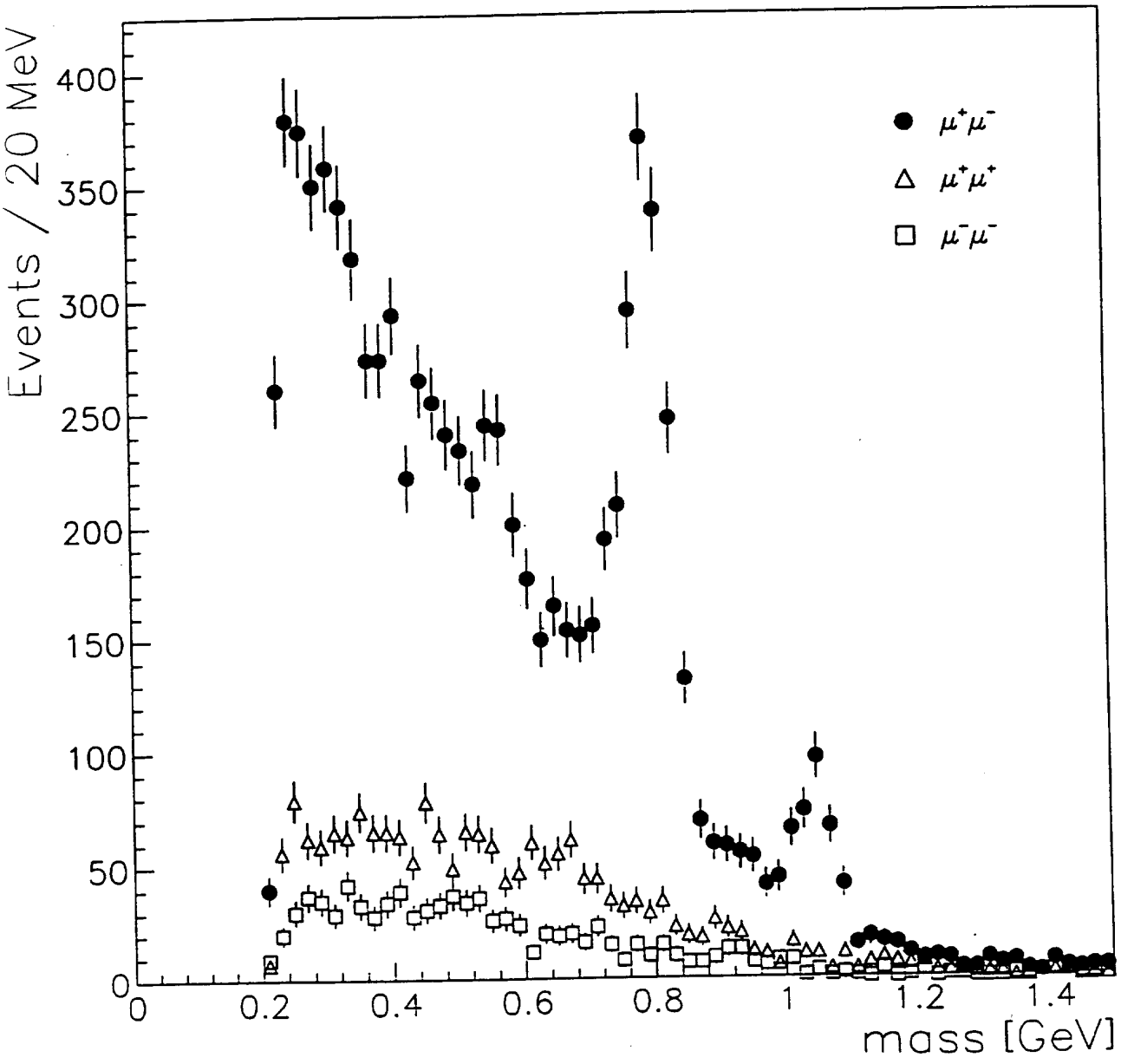

Figure 7: Mass spectrum of final sample of di-muon events. Full circles: $\mu^+\mu^-$; Open triangles and squares: $\mu^+\mu^+$ and $\mu^-\mu^-$.

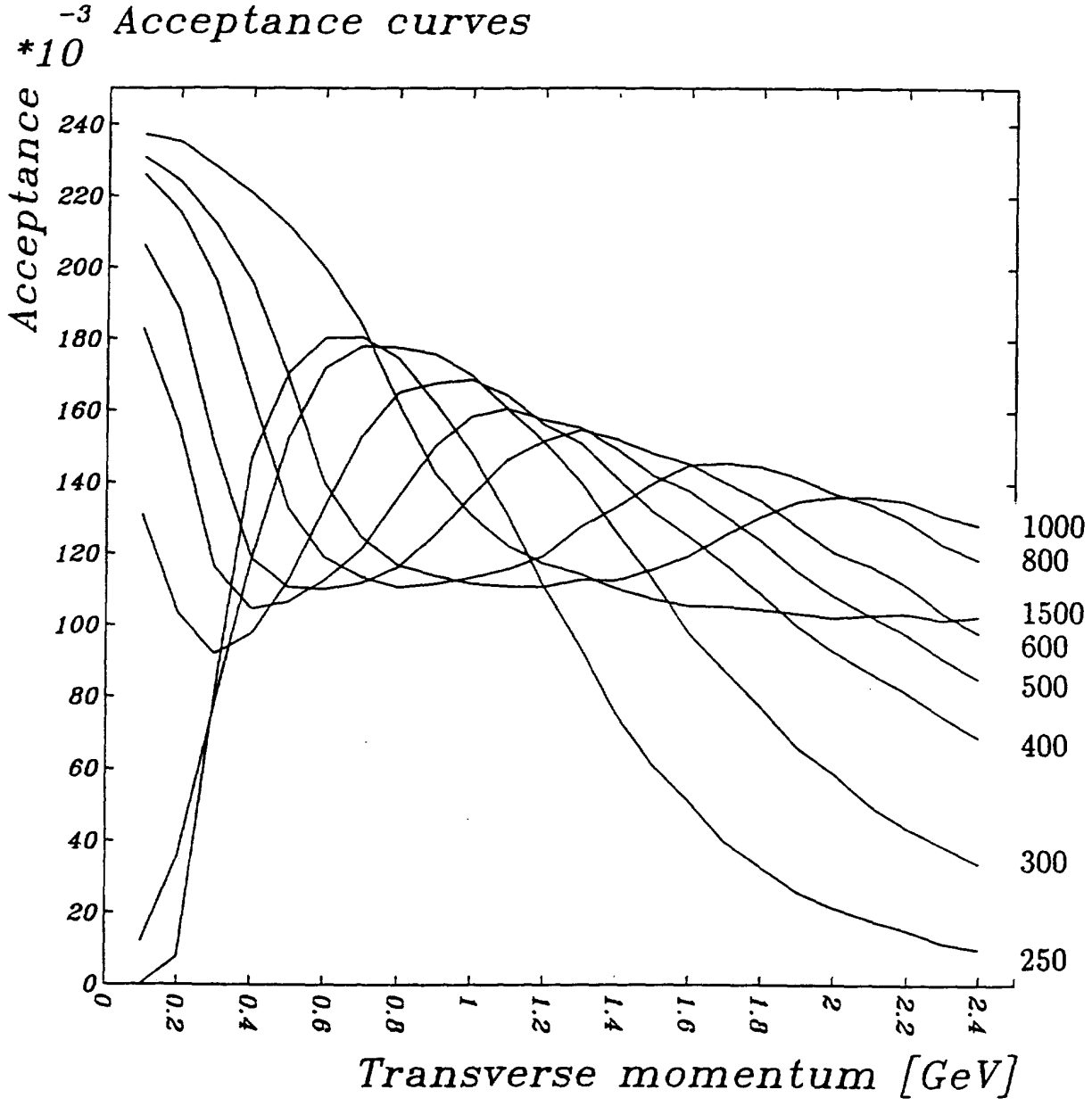

Figure 8: Acceptance for muon pairs as a function of p_T for pair masses of 250, 300, 400, 500, 600, 800, 1000, and 1500 MeV. The pair is produced at $y = 1$ and decays with $cos\theta^* = 0$. At $p_T \sim 0.1$ GeV the lowest acceptance is for mass of 250 MeV and the highest for mass of 1500 MeV. The acceptance includes the effect of the reconstruction efficiency.

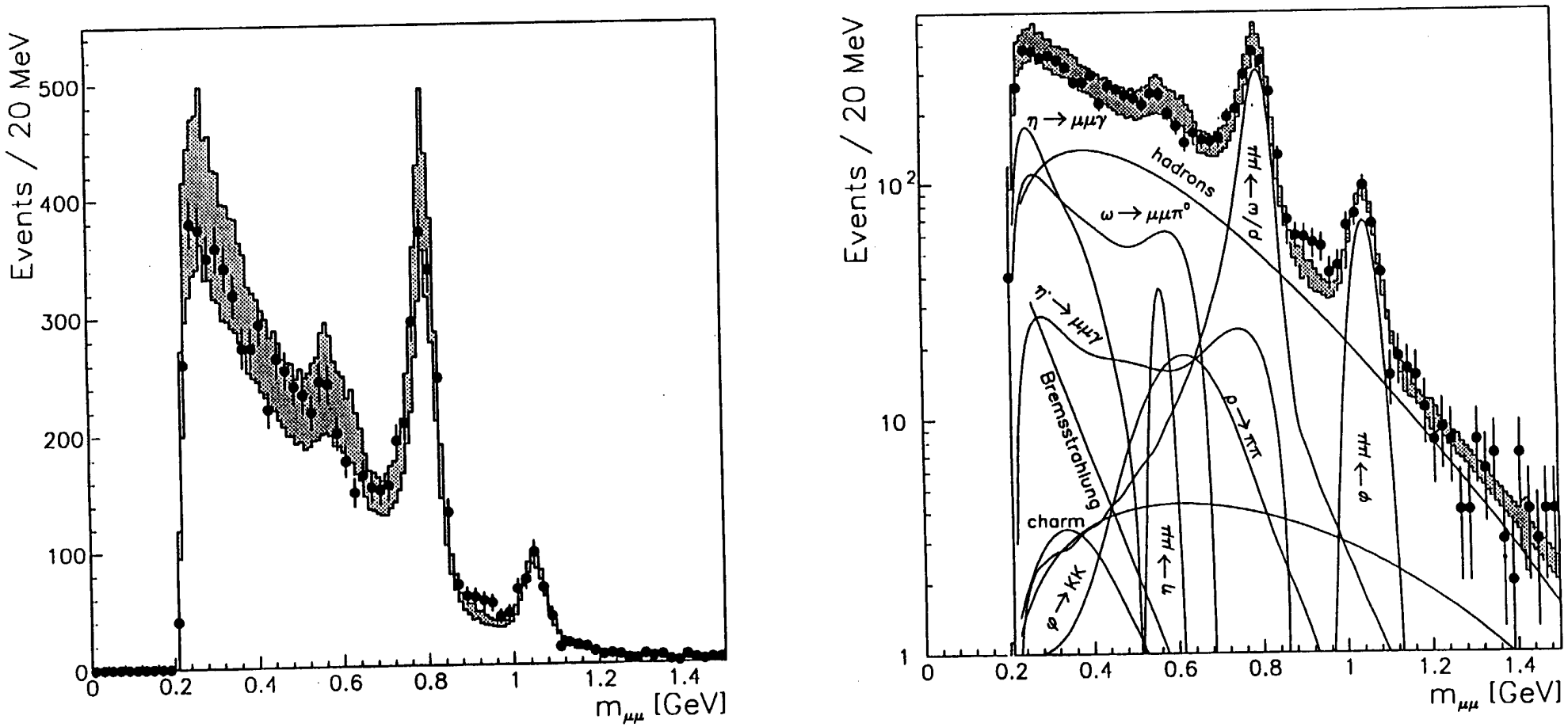

Figure 9: Mass spectrum of di-muon events showing the data (full circles) and the various contributions.
a) Linear scale showing the sum of all individual contributions;
b) Logarithmic scale showing the individual contributions as well.
The shaded region indicates the $\pm 1\sigma$ error on the summed contributions. Data are not corrected for acceptance; acceptance effects are included in the predictions.

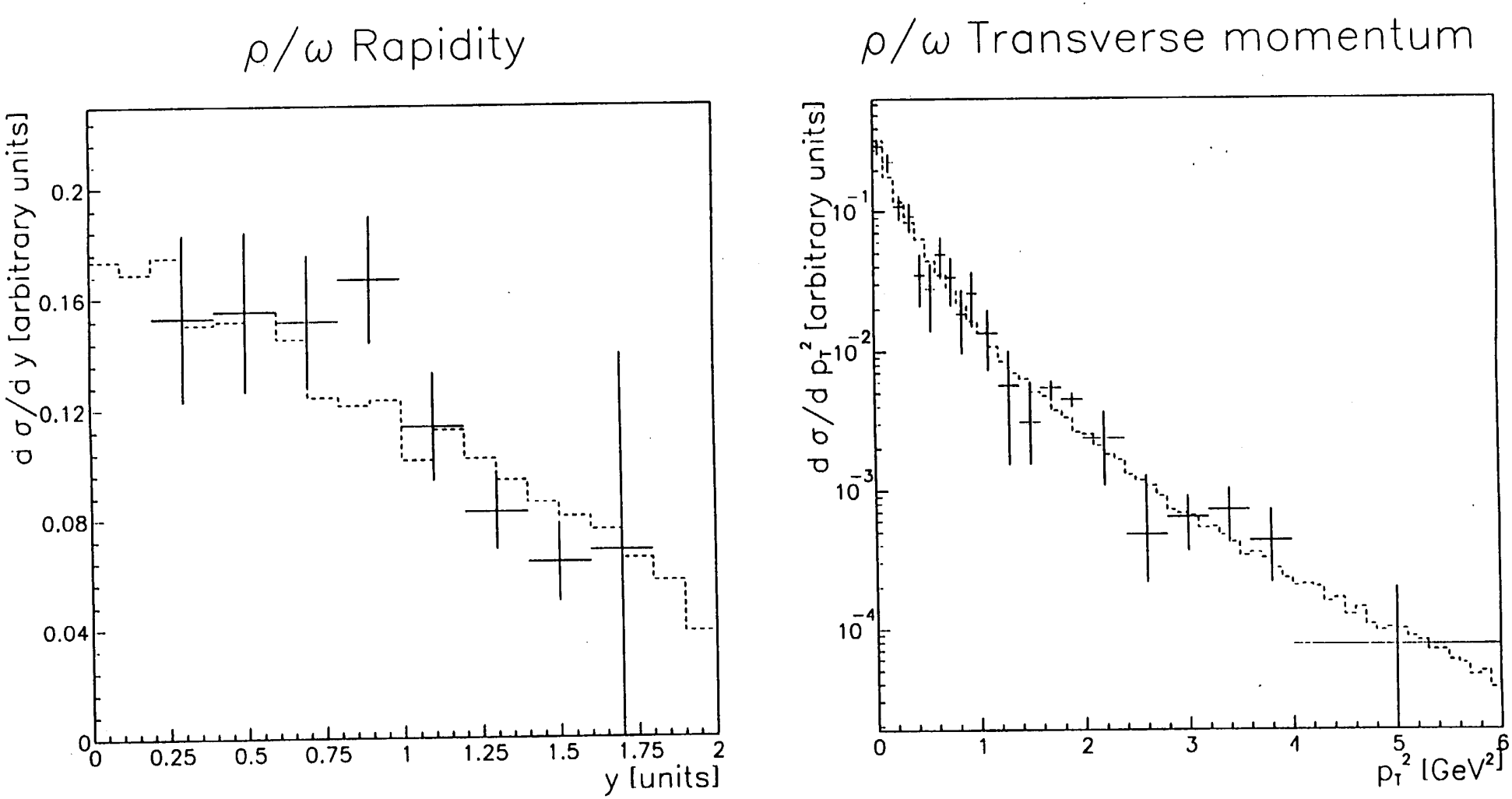

Figure 10: Distributions in y and p_T for $\mu^+\mu^-$ pairs in the mass range $0.6-0.9$ GeV, which is dominated by the ρ/ω. The contribution from π and K decays has been subtracted. The data are described very well by the B-G parametrisation (dashed line).

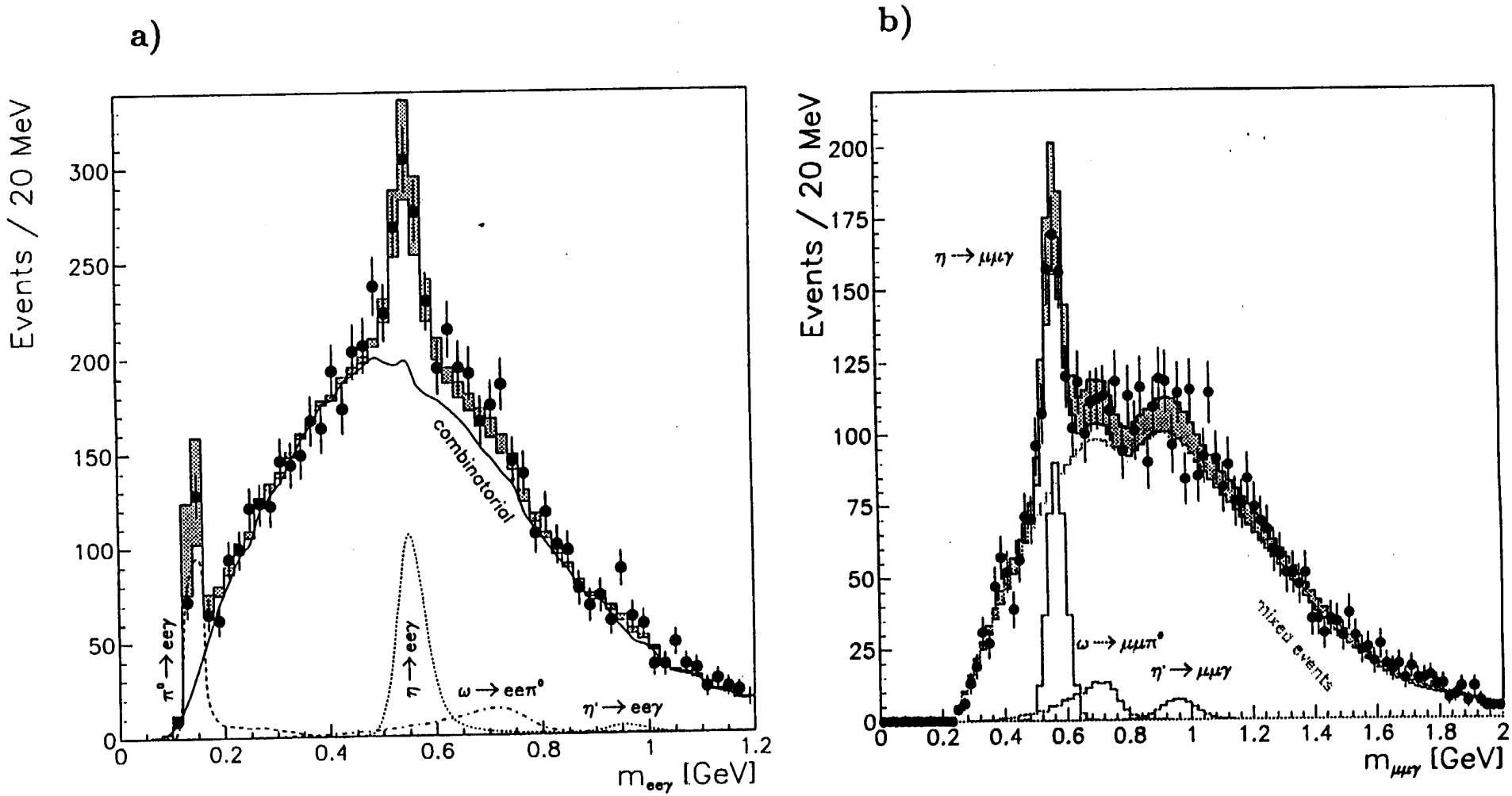

Figure 11: Distributions of a) $e^+e^-\gamma$ and b) $\mu^+\mu^-\gamma$ events. The η is clearly visible through its $l^+l^-\gamma$ decay channel. The fit is described in the text.

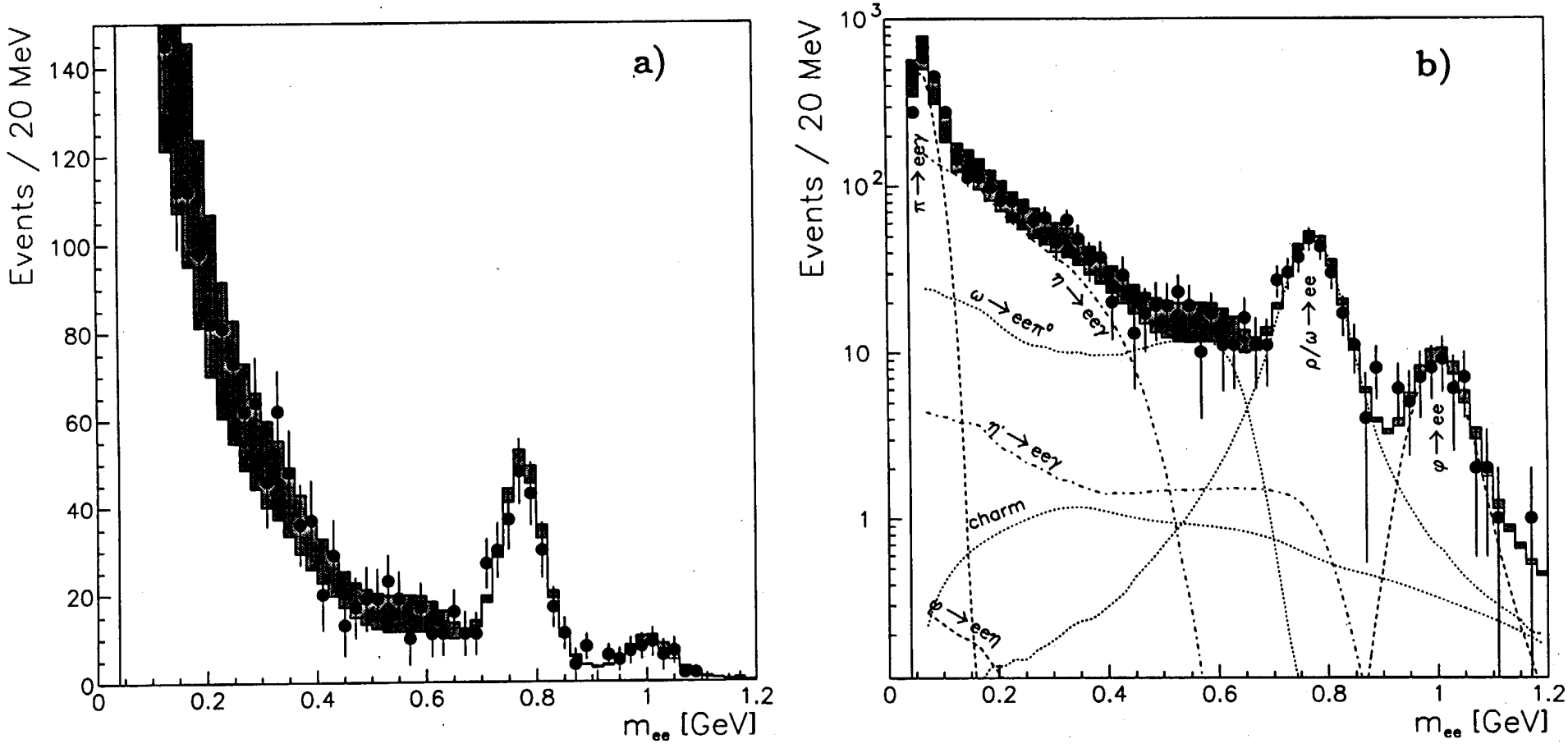

Figure 12: Mass spectrum of di-electron events showing the data (full circles) and the various contributions.
a) Linear scale showing the sum of all individual contributions;
b) Logarithmic scale showing the individual contributions as well.
The shaded region indicates the $\pm 1\sigma$ error on the summed contributions. Data are not corrected for acceptance; acceptance effects are included in the predictions.

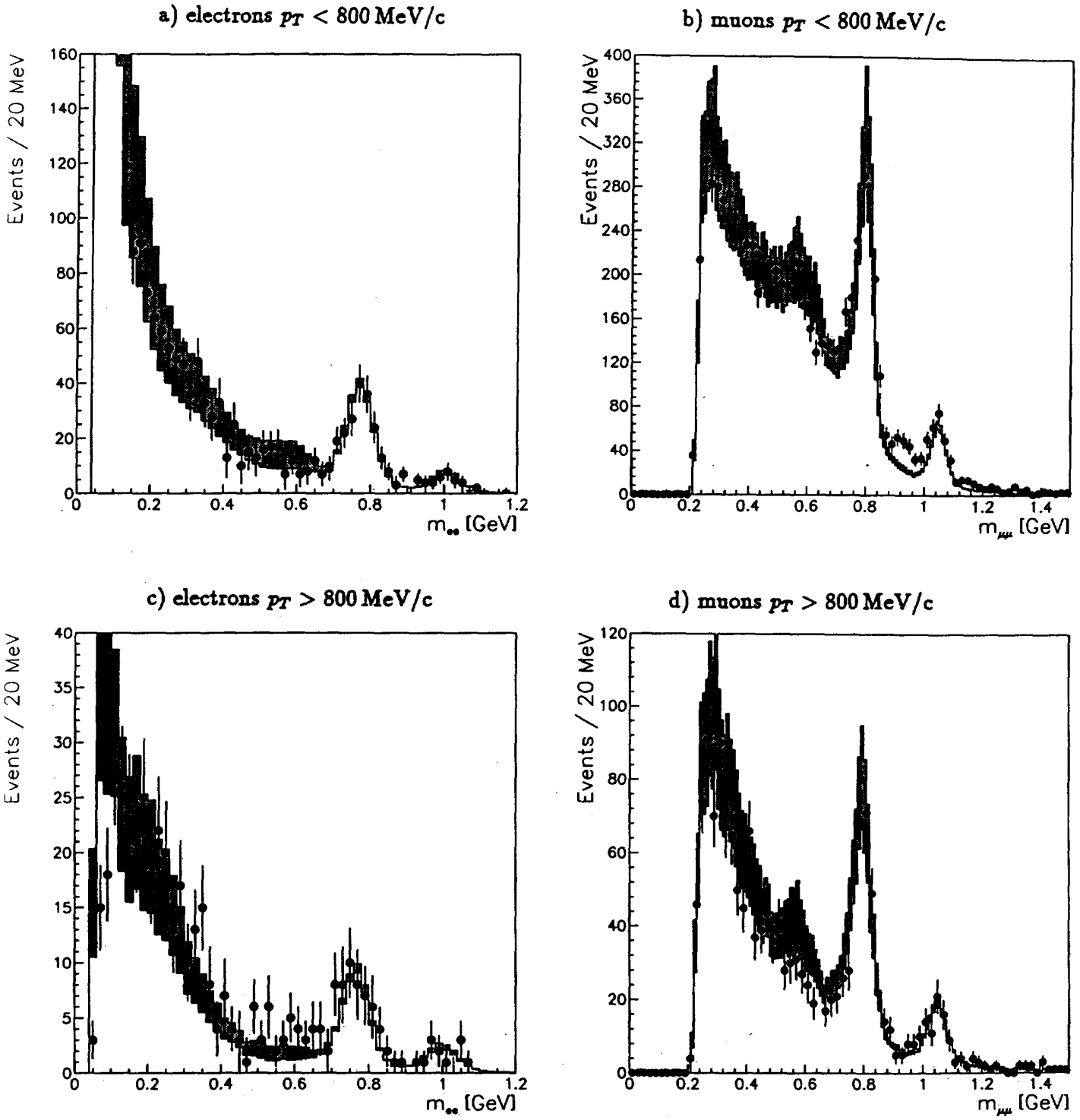

Figure 13: Mass spectrum of di-electron and di-muon events for $p_T < 800\,\mathrm{MeV/c}$ and $p_T > 800\,\mathrm{MeV/c}$. The shaded region indicates the $\pm 1\sigma$ error on the sum of all contributions. Data are not corrected for acceptance; acceptance effects are included in the predictions.

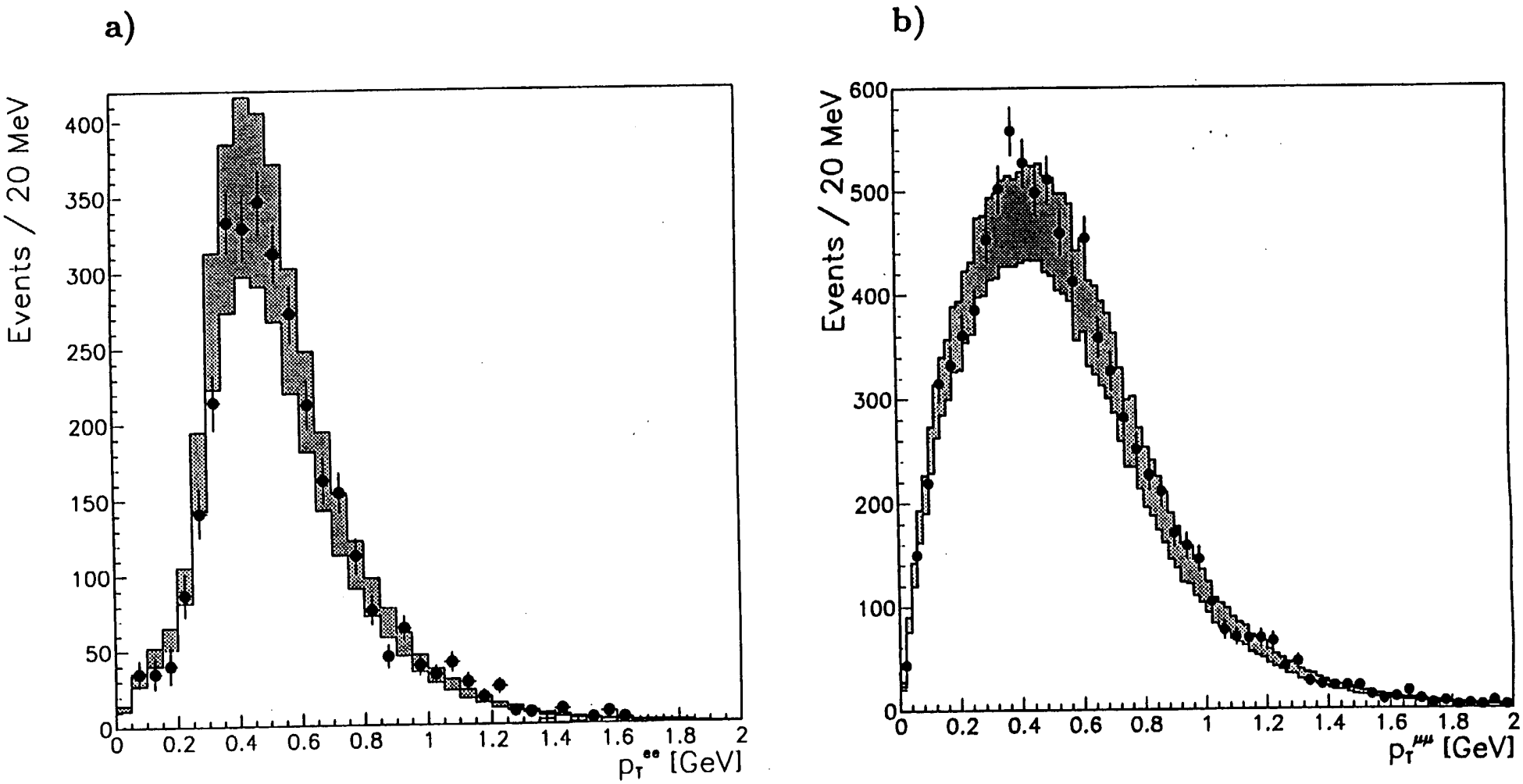

Figure 14: p_T spectrum of a) di-electron and b) di-muon events. The shaded region indicates the $\pm 1\sigma$ error on the sum of all contributions. Data are not corrected for acceptance; acceptance effects are included in the predictions.

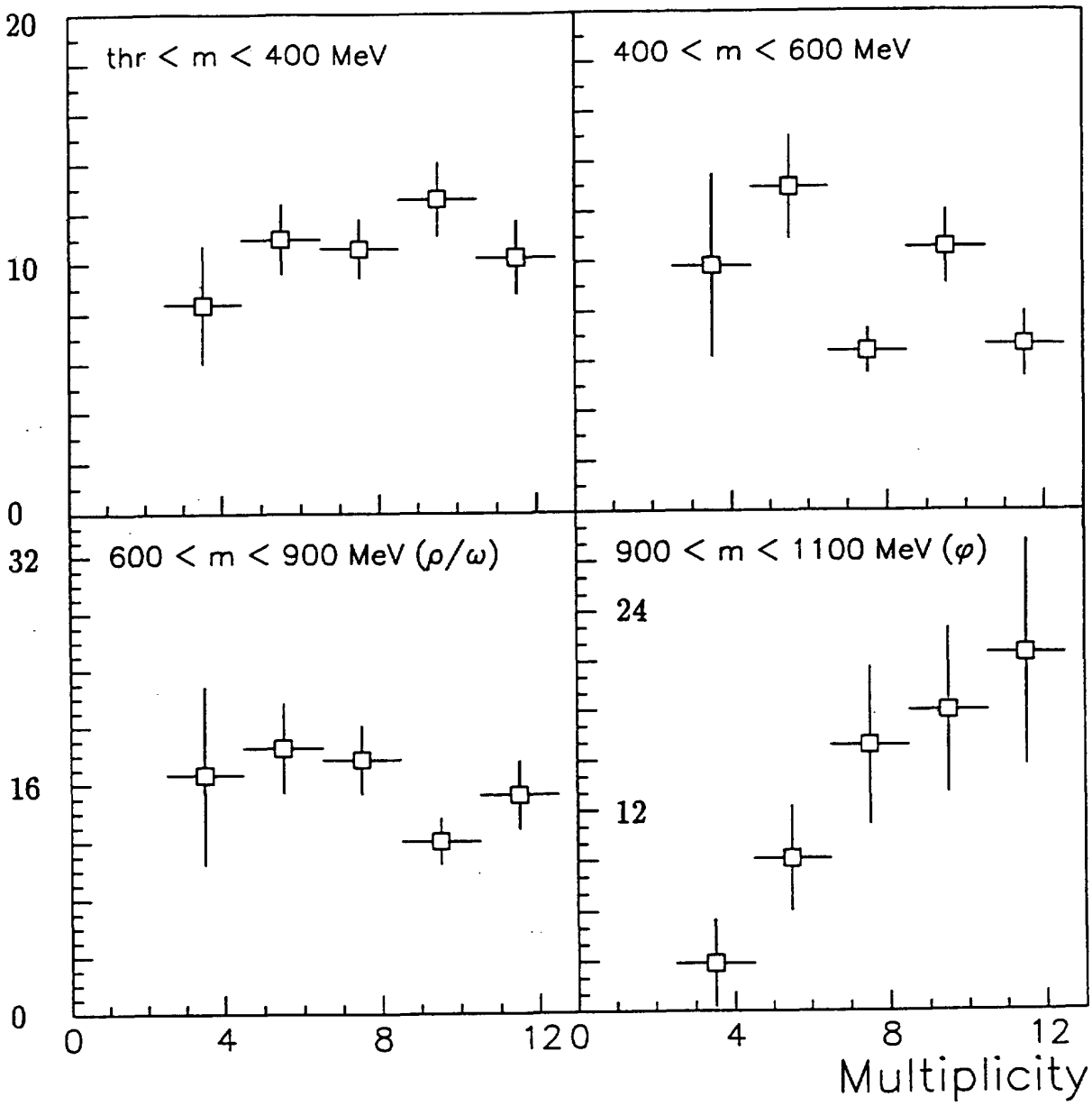

Figure 15: The quantity H as a function of multiplicity for muon pairs for four different mass intervals. (H is defined in the text.)